

# Genome-wide inference of ancestral recombination graphs

Matthew D. Rasmussen<sup>\*,†</sup>, Adam Siepel<sup>\*</sup>

Department of Biological Statistics and Computational Biology, Cornell University, Ithaca, New York 14853, USA

## \*Corresponding authors:

Matthew D. Rasmussen, Adam Siepel

102 Weill Hall

Ithaca, NY 14853, USA

E-mail: rasmussen@cornell.edu, acs4@cornell.edu

<sup>†</sup>**Current address:** Counsyl, 180 Kimball Way, South San Francisco, CA 94080, USA

**Keywords:** population genomics, sequentially Markov coalescent, hidden Markov model, Markov chain Monte Carlo, Bayesian phylogenetics

**Running title:** Genome-wide ARG inference

## Abstract

The complex correlation structure of a collection of orthologous DNA sequences is uniquely captured by the “ancestral recombination graph” (ARG), a complete record of all coalescence and recombination events in the history of the sample. However, existing methods for ARG inference are extremely computationally intensive, depend on fairly crude approximations, or are limited to small numbers of sequences. As a consequence, explicit ARG inference is rarely used in applied population genomics. Here, we introduce a new algorithm for ARG inference that is efficient enough to be applied on the scale of dozens of complete human genomes. The key idea of our approach is to sample an ARG of  $n$  chromosomes conditional on an ARG of  $n - 1$  chromosomes, an operation we call “threading”. Using techniques based on hidden Markov models, this threading operation can be performed exactly, up to the assumptions of the sequentially Markov coalescent and a discretization of time. An extension allows for threading of subtrees instead of individual sequences. Repeated application of these threading operations results in highly efficient Markov chain Monte Carlo samplers for ARGs. We have implemented these methods in a computer program called *ARGweaver*. Experiments with simulated data indicate that *ARGweaver* converges rapidly to the true posterior distribution and is effective in recovering various features of the ARG, for twenty or more sequences generated under realistic parameters for human populations. We also report initial results from applications of *ARGweaver* to high-coverage individual human genome sequences from Complete Genomics. We show that several features of the inferred ARGs—including recombination rates, times to most recent common ancestry, and local effective population sizes—show expected patterns across the genome. In addition, even when a noninformative prior is assumed, the inferred ARGs can be used to reconstruct population phylogenies with reasonable accuracy. Finally, we present a novel approach for visualization of genome-wide ARGs. Work is in progress on further applications of these methods to genome-wide sequence data.

# Introduction

At each genomic position, orthologous DNA sequences drawn from one or more populations are related by a combinatorial object known as a genealogy, or gene tree. Historical recombination events lead to changes in these genealogies from one genomic position to the next. The resulting structure—essentially, a collection of correlated trees (see [1, 2])—is unwieldy, analytically intractable, and poorly approximated by standard representations of high-dimensional data. These unique properties of genetic data have inspired numerous innovative techniques for probabilistic modeling and statistical inference over a period of many decades [3–9]. More recently, they have led to creative approaches that achieve computational tractability by operating on various summaries of the data [10–18]. However, these approaches do not fully capture the correlation structure of collections of DNA sequences, which inevitably leads to limitations in power, accuracy, and generality.

In principle, the correlation structure of a collection of colinear orthologous sequences can be fully described using a data structure known as the *ancestral recombination graph* (ARG) [19, 20]. The ARG (see example in Figure 1A) provides a record of all coalescence and recombination events since the divergence of the sequences under study. It specifies a complete genealogy at each position along a sequence and gives the locations and times of all recombination events. In many senses, the ARG is the ideal data structure for population genomic analysis. Indeed, if an accurate ARG could be obtained, many problems of interest today—such as the estimation of recombination rates or ancestral effective population sizes—would become trivial. Many other problems—such as the estimation of population divergence times or rates of gene flow between populations, or the detection of selective sweeps—would be greatly simplified. Essentially all other widely used data representations, including the site frequency spectrum, principle components, haplotype maps, and identity by descent spectra, can be thought of as low-dimensional summaries of the ARG and are strictly less informative.

It is relatively straightforward to extend the widely used coalescent framework for describing genealogies [9] to include recombination, and the resulting *coalescent-with-recombination* (CwR) [21] is regarded as an adequately rich generative process for ARGs in most settings of interest. However, inferring an ARG from sequence data under the CwR is a notoriously difficult problem. Furthermore, the data are generally only weakly informative about the ARG, so it is often desirable to regard it as a “nuisance” variable to be integrated out in likelihood calculations (e.g., [22]). During the past decade and a half, various attempts have been made to perform statistical inference of ARGs, using techniques such as importance sampling [22, 23] and Markov chain Monte Carlo sampling [24–27]. There is also a considerable literature on the use of heuristic or approximate methods for ARG reconstruction in a parsimony framework [28–35]. However, while several of these approaches have shown promise, they are generally highly computationally intensive and/or limited in accuracy, and they are not suitable for application to large-scale data sets. As a result, explicit ARG inference is rarely used today in applied population genomics.

The CwR is conventionally described as a stochastic process in time [21], but Wiuf and Hein [36] showed that it could be reformulated as a mathematically equivalent process along the genome sequence. Unlike the process in time, this “sequential” process is not Markovian, that is, the genealogies for genomic positions  $1, \dots, i-1$  cannot be “forgotten” when generating the genealogy for position  $i+1$  based on the genealogy for position  $i$ . The reason is that

long-range dependencies are induced by so-called “trapped” sequences (genetic material nonancestral to the sample that is flanked by segments that are ancestral). Nevertheless, the process can be precisely described by keeping track not just of the genealogy at position  $i$ , but of an expanded graph that includes nonancestral lineages. However, McVean and Cardin [37] showed that a simulation process that simply disregarded the non-Markovian features of the sequential process resulted in collections of sequences that were remarkably consistent in most respects with those generated by the full CwR. In other words, the CwR is almost Markovian, in the sense that the long-range correlations induced by trapped material are fairly weak and have a minimal impact on the data. This approximation to the full process, called the *sequentially Markov coalescent* (SMC), was later extended to a process known as the SMC', which further improves the fit to the data by allowing for an additional class of recombinations [38].

In recent years, the SMC has become favorite starting point for approximate methods for statistical inference of ARGs [39–42]. The key insight behind these methods is that, if the continuous state space for the Markov chain (i.e., the set of all possible genealogies) is approximated by a finite set that is not too large—typically by enumerating tree topologies and/or discretizing time—then inference can be performed efficiently using well-known algorithms for hidden Markov models (HMMs). Perhaps the simplest and most elegant example of this approach is the pair-wise sequentially Markov coalescent (PSMC) of Li and Durbin [42]. This method applies to pairs of homologous chromosomes (typically the two chromosomes in a diploid individual) and is used to reconstruct a profile of effective population sizes over time. In this case, there is only one possible tree topology and one coalescence event to consider at each genomic position, so it is sufficient to discretize time and allow for coalescence within any of  $k$  possible time slices. Using the resulting  $k$ -state HMM, it is possible to perform inference integrating over all possible coalescent and recombination histories (i.e., all possible ARGs). A similarly elegant HMM-based approach has been used to estimate ancestral effective population sizes and divergence times from individual representatives of small numbers of closely related species [39–41]. Because of their dependency on a complete characterization of the SMC state space, however, these methods have the important restriction that they can only be applied to small numbers of samples. This limits their utility with newly emerging population genomic datasets and leads to reduced power for certain features of interest, such as recent effective population sizes, recombination rates, or local signatures of natural selection.

An alternative modeling approach, with better scaling properties, is the product of approximate conditionals (PAC) or “copying” model of Li and Stephens [43] (see also [22, 44]). The PAC model is motivated primarily by computational tractability and is not based on an explicit evolutionary model. The model generates the  $n$ th sequence in a collection by concatenating (noisy) copies of fragments of the previous  $n - 1$  sequences. The source of each copied fragment represents the “closest” (most recently diverged) genome for that segment, and the noise process allows for mutations since the source and destination copies diverged. The PAC framework has been widely used in many applications in statistical genetics, including recombination rate estimation, local ancestry inference, haplotype phasing, and genotype imputation (e.g., [45–49]), and it generally offers good performance at minimal computational cost. Recently, Song and colleagues have generalized this framework to make use of conditional sampling distributions (CSDs) based on models closely related to, and in some cases equivalent to, the SMC [50–53]. They have demonstrated improved accuracy in conditional likelihood calculations [50, 51] and have shown that their methods can be

effective in demographic inference [52, 53]. However, this approach avoids explicit ARG inference and therefore can only be used to characterize properties of the ARG that are directly determined by model parameters, which somewhat limits its breadth of application (see Discussion).

In this paper, we introduce a new, more general algorithm for ARG inference that combines many of the benefits of the small-sample SMC-based approaches and the large-sample CSD-based methods. Like the PSMC, our algorithm requires no approximations beyond those of the SMC and a discretization of time, but it improves on the PSMC by allowing multiple genome sequences to be considered simultaneously. The key idea of our approach is to sample an ARG of  $n$  sequences conditional on an ARG of  $n - 1$  sequences, an operation we call “threading.” Using HMM-based methods, we can efficiently sample new threadings from the exact conditional distribution of interest. By repeatedly removing and re-threading individual sequences, we obtain an efficient Gibbs sampler for ARGs. We show how to improve this basic Gibbs sampler by including operations that rethread entire subtrees rather than individual sequences. Using simulated data, we show that our Markov chain Monte Carlo sampler mixes well and is able to recover many properties of the true ARG with good accuracy. In addition, we apply our methods to whole-genome sequence data for human populations from Complete Genomics and provide demonstrations of their potential applicability to several problems of interest, including demography inference, the detection of natural selection, and the estimation of recombination rates. We also demonstrate new methods for visualization of ARGs on a genomic scale.

## Results

### Generative Model

#### The Sequentially Markov Coalescent

The starting point for our model is the Sequentially Markov Coalescent (SMC) introduced by McVean and Cardin [37]. We begin by briefly reviewing the SMC and introducing notation that will be useful below in describing a general discretized version of this model.

The SMC is a stochastic process for generating a sequence of local trees,  $T^n = T_1^n, \dots, T_m^n$  and corresponding genomic breakpoints  $\mathbf{b} = b_1, \dots, b_{m+1}$ , such that each  $T_i^n$  ( $1 \leq i \leq m$ ) describes the ancestry of a collection of  $n$  sequences in a nonrecombining genomic interval  $[b_i, b_{i+1})$ , and each breakpoint  $b_i$  between intervals  $T_{i-1}^n$  and  $T_i^n$  corresponds to a recombination event (Figure 1B). The model is continuous in both space and time, with each node  $v$  in each  $T_i^n$  having a real-valued age  $t(v) \geq 0$  in generations ago, and each breakpoint  $b_i$  falling in the continuous interval  $[0, L]$ , where  $L$  is the total length of the genomic segment of interest in nucleotide sites. The intervals are mutually exclusive and nonoverlapping, with  $b_1 = 0$ ,  $b_{m+1} = L$ , and  $b_i < b_{i+1}$  for all  $i$ . Each  $T_i^n$  is a binary tree with  $t(v) = 0$ , for all leaf nodes  $v$ , and has a marginal distribution given by the standard coalescent. We will use the convention of indexing branches in the trees by their descendant nodes; that is, branch  $v$  is the branch between node  $v$  and its parent.

As shown by Wiuf and Hein [36], the correlation structure of the local trees and recombinations under the full CwR

is complex. The SMC approximates this distribution by assuming that  $T_i^n$  is conditionally independent of  $T_1^n, \dots, T_{i-2}^n$  given  $T_{i-1}^n$ , and, similarly, that  $b_i$  depends only on  $b_{i-1}$  and  $T_{i-1}^n$ , so that,

$$P(\mathbf{T}^n, \mathbf{b} \mid N, \rho) = P(T_1^n \mid N) \left[ \prod_{i=2}^m P(b_i \mid b_{i-1}, T_{i-1}^n) P(T_i^n \mid T_{i-1}^n, N, \rho) \right] P(b_{m+1} = L \mid b_m, T_m^n), \quad (1)$$

where  $N$  is the effective population size,  $\rho$  is the recombination rate, and it is understood that  $b_1 = 0$ . Thus, the SMC can be viewed as generating a sequence of local trees and corresponding breakpoints by a first-order Markov process. The key to the model is to define the conditional distributions  $P(b_i \mid b_{i-1}, T_{i-1}^n)$  and  $P(T_i^n \mid T_{i-1}^n, N, \rho)$  such that this Markov process closely approximates the coalescent-with-recombination. Briefly, this is accomplished by first sampling the initial tree  $T_1^n$  from the standard coalescent and setting  $b_1 = 0$ , and then iteratively (i) determining the next breakpoint,  $b_i$ , by incrementing  $b_{i-1}$  by an exponential random variate with rate  $\rho|T_{i-1}^n|$ , where  $|T_{i-1}^n|$  denotes the total branch length of  $T_{i-1}^n$ ; (ii) sampling a recombination point  $R_i = (w_i, u_i)$  uniformly along the branches beneath the root of  $T_{i-1}^n$ , where  $w_i$  is a branch and  $u_i$  is a time along that branch; (iii) dissolving the branch  $w_i$  above point  $u_i$ ; and (iv) allowing  $w_i$  to rejoin the remainder of tree  $T_{i-1}^n$  above time  $u_i$  by the standard coalescent process, creating a new tree  $T_i^n$  (Figure 1B). As a generative process for an arbitrary number of genomic segments, the SMC can be implemented by simply repeating the iterative process until  $b_i \geq L$ , then setting  $m$  equal to  $i - 1$  and  $b_{m+1}$  equal to  $L$ .

Notice that, if the sampled recombination points  $R_i$  are retained, this process generates not only a sequence of local trees but a complete ARG. In addition, a sampled sequence of local trees,  $\mathbf{T}^n$ , is sufficient for generation of  $n$  aligned DNA sequences corresponding to the leaves of the trees (Figure 1C). Augmented in this way, the SMC can be considered a full generative model for ARGs and sequence data.

### The Discretized Sequentially Markov Coalescent

We now define an approximation of the SMC that is discrete in both space and time, which we call the Discretized Sequentially Markov Coalescent (DSMC). The DSMC can be viewed as a generalization to multiple genomes of the discretized pairwise sequentially Markov coalescent (PSMC) used by Li and Durbin [42]. It is also closely related to several other recently described discretized Markovian coalescent models [39, 40, 51].

The DSMC assumes that time is partitioned into  $K$  intervals, whose boundaries are given by a sequence of time points  $\mathcal{P} = (s_0, \dots, s_K)$ , with  $s_0 = 0$ ,  $s_{j+1} > s_j$  for all  $j$  ( $0 \leq j < K$ ), and  $s_K$  equal to a user-specified maximum value. Every coalescence or recombination event is assumed to occur precisely at one of these  $K + 1$  time points. Various strategies can be used to determine these time points (see, e.g., [51]). We simply distribute them uniformly on a logarithmic scale, so that the resolution of the discretization scheme is finest near the leaves of the ARG, where the density of events is expected to be greatest (see Methods). Each local block is assumed to have an integral length measured in base pairs, with all recombinations occurring between adjacent nucleotides. The DSMC approaches the SMC as the number of intervals  $K$  and the sequence length  $L$  grow large, for fixed  $N$  and  $\rho$ .

Like the SMC, the DSMC generates an ARG  $G^n$  for  $n$  (haploid) sequences, each containing  $L$  nucleotides (Figure 1B). In the discrete setting, it is convenient to define local trees and recombination events at the level of individual

nucleotide positions. Assuming that  $R_i^n$  denotes a recombination between  $T_{i-1}^n$  and  $T_i^n$ , we write  $G^n = (T^n, R^n)$ , with  $T^n = (T_1^n, \dots, T_L^n)$  for positions  $1, \dots, L$ , and  $R^n = (R_2^n, \dots, R_L^n)$ . Notice that it is possible in this setting that  $R_i^n = \emptyset$  and  $T_i^n = T_{i-1}^n$ . Where a recombination occurs ( $R_i^n \neq \emptyset$ ), we write  $R_i^n = (w_i, u_i)$  where  $w_i$  is the branch in  $T_{i-1}^n$  and  $u_i \in \mathcal{P}$  is the time point of the recombination. For simplicity and computational efficiency, we assume that at most one recombination occurs between each pair of adjacent sites. Given the sparsity of variant sites in most data sets, this simplification is likely to have, at most, a minor effect during inference (see Discussion).

Like the SMC, the DSMC can additionally be used to generate an alignment of DNA sequences (Figure 1C). We denote such an alignment by  $D^n = (D_1^n, \dots, D_L^n)$ , where each  $D_i^n$  represents an alignment column of height  $n$ . Each  $D_i^n$  can be generated, in the ordinary way, by sampling an ancestral allele from an appropriate background distribution, and then allowing this allele to mutate stochastically along the branches of the corresponding local tree, in a branch-length-dependent manner. We denote the induced conditional probability distribution over alignment columns by  $P(D_i^n | T_i^n, \mu)$ , where  $\mu$  is the mutation rate. In this work, we assume a Jukes-Cantor model [54] for nucleotide mutations along the branches of the tree, but another mutation model can easily be used instead. Notice that, while the recombinations  $R^n$  are required to define the ARG completely, the probability of the sequence data given the ARG depends only on the local trees  $T^n$ .

## Inference Strategy

### Hidden Markov Model

In the case of an observed alignment,  $D^n$  and an unobserved ARG,  $G^n = (T^n, R^n)$ , the DSMC can be viewed as a hidden Markov model (HMM), with a state space given by all possible local trees, transition probabilities given by the conditional distributions  $P(T_i^n | T_{i-1}^n, \rho, N)$ , and emission probabilities given by the conditional distributions for alignment columns,  $P(D_i^n | T_i^n, \mu)$  (see Methods). However, this naive formulation is impractical as a framework for inference, because the set of possible local trees—and hence the state space—grows super-exponentially with  $n$ . Even with additional assumptions, similar approaches have only been able to accommodate small numbers of sequences [32, 35, 55].

Instead, we use an alternative strategy with better scaling properties. The key idea of our approach is to sample the ancestry of only one sequence at a time, while conditioning on the ancestry of the other  $n - 1$  sequences. Repeated applications of this “threading” operation form the basis of a Markov chain Monte Carlo sampler that explores the posterior distribution of ARGs. In essence, the threading operation adds one branch to each local tree in a manner that is consistent with the assumed recombination process and the observed data (Figure 2). While conditioning on a given set of local trees introduces a number of technical challenges, the Markovian properties of the DSMC are retained in the threading problem, and it can be solved using standard dynamic programming algorithms for HMMs.

## The Threading Problem

The threading problem can now be precisely described as follows. Assume we are given an ARG for  $n-1$  sequences,  $\mathbf{G}^{n-1}$ , a corresponding data set  $\mathbf{D}^{n-1}$ , and a set of model parameters  $\Theta = (\mu, \rho, N)$ . Assume further that  $\mathbf{G}^{n-1}$  is consistent with the assumptions of the DSMC (for example, all of its recombination and coalescent events occur at time points in  $\mathcal{P}$  and it contains at most one recombination per position). Finally, assume that we are given an  $n$ th sequence  $d$ , of the same length of the others, and let  $\mathbf{D}^n = (\mathbf{D}^{n-1}, d)$ . The threading problem is to sample a new ARG  $\mathbf{G}^n$  from the conditional distribution  $P(\mathbf{G}^n | \mathbf{G}^{n-1}, \mathbf{D}^n, \Theta)$  under the DSMC.

The problem is simplified by recognizing that  $\mathbf{G}^n$  can be defined by augmenting  $\mathbf{G}^{n-1}$  with the additional recombination and coalescence events required for the  $n$ th sequence. First, let  $\mathbf{G}^{n-1}$  be represented in terms of its local trees and recombination points:  $\mathbf{G}^{n-1} = (\mathbf{T}^{n-1}, \mathbf{R}^{n-1})$ . Now, observe that specifying the new coalescence events in  $\mathbf{G}^{n-1}$  is equivalent to adding one branch to each local tree,  $T_i^{n-1}$  for  $i \in \{1, \dots, L\}$ , to obtain a new tree  $T_i^n$  (Figure 2). Let us denote the point at which each of these new branches attaches to the smaller subtree at each genomic position  $i$  by  $y_i = (x_i, t_i)$ , where  $x_i$  indicates a branch in  $T_i^{n-1}$  and  $t_i \in \mathcal{P}$  indicates the coalescence time along that branch. Thus, the *coalescence threading* of the  $n$ th sequence is given by the sequence  $\mathbf{Y} = (y_1, \dots, y_L)$ .

To complete the definition of  $\mathbf{G}^n$ , we must also specify the precise locations of the additional recombinations associated with the threading—that is, the specific time point at which each branch in a local tree  $T_{i-1}$  was broken before the branch was allowed to re-coalesce in a new location in tree  $T_i$ . Here it is useful to partition the recombinations into those that are given by  $\mathbf{G}^{n-1}$ , denoted  $\mathbf{R}^{n-1}$ , and those new to  $\mathbf{G}^n$ , which we denote  $\mathbf{Z} = (z_1, \dots, z_L)$  (Figure 3A&B). Each  $z_i$  is either null ( $z_i = \emptyset$ ), meaning that there is no new recombination between  $T_{i-1}^n$  and  $T_i^n$ , or defined by  $z_i = (w_i, u_i)$ , where  $w_i$  is a branch in  $T_{i-1}^n$  and  $u_i \in \mathcal{P}$  is the time along that branch at which the recombination occurred. We call  $\mathbf{Z}$  the *recombination threading* of the  $n$ th sequence. Our approach is first to sample the coalescence threading  $\mathbf{Y}$  and then to sample the recombination threading  $\mathbf{Z}$  conditional on  $\mathbf{Y}$ . This separation into two sampling steps allows for a substantially reduced state space in the coalescence threading operation, leading to significant savings in computation. When sampling the coalescence threading, we integrate over the locations of the new recombinations  $\mathbf{Z}$ , as in previous work [42, 51]. The second step can be accomplished in a straightforward manner independently for each recombination event, by taking advantage of the conditional independence structure of the DSMC model (see Methods for details).

The core problem, then, is to sample the coalescence threading  $\mathbf{Y}$  from the distribution,

$$\begin{aligned} P(\mathbf{Y} | \bar{\mathbf{T}}^{n-1}, \bar{\mathbf{R}}^{n-1}, \bar{\mathbf{D}}^n, \Theta) &\propto P(\mathbf{Y}, \bar{\mathbf{T}}^{n-1}, \bar{\mathbf{R}}^{n-1}, \bar{\mathbf{D}}^n | \Theta) \\ &= P(\bar{\mathbf{T}}_1^{n-1}, y_1 | N) P(\bar{\mathbf{D}}_1 | \bar{\mathbf{T}}_1^{n-1}, y_1, \mu) \prod_{i=2}^L P(\bar{\mathbf{R}}_i^{n-1}, \bar{\mathbf{T}}_i^{n-1}, y_i | \bar{\mathbf{T}}_{i-1}^{n-1}, y_{i-1}, \rho, N) P(\bar{\mathbf{D}}_i | \bar{\mathbf{T}}_i^{n-1}, y_i, \mu), \end{aligned} \quad (2)$$

where the notation  $\bar{A}$  indicates that random variable  $A$  is held fixed (“clamped”) at a particular value throughout the procedure. This equation defines a hidden Markov model with a state space given by the possible values of each  $y_i$ , transition probabilities given by  $a_{l,m}^i = P(\bar{\mathbf{R}}_i^{n-1}, \bar{\mathbf{T}}_i^{n-1}, y_i = m | \bar{\mathbf{T}}_{i-1}^{n-1}, y_{i-1} = l, \rho, N)$  and emission probabilities given

by  $b_i^j(D_i^n) = P(D_i | \bar{T}_i^{n-1}, y_i = l, \mu)$  (Figure 3C). Notice that the location of the new recombination,  $z_i$ , is implicitly integrated out in  $a_{i,m}^j$ . Despite some unusual features of this model—for example, it has a heterogenous state space and normalization structure along the sequence—its Markovian dependency structure is retained, and the problem of drawing a coalescent threading  $Y$  from the desired conditional distribution can be solved exactly by dynamic programming using the stochastic traceback algorithm for HMMs (see Methods for details).

## Markov chain Monte Carlo sampling

The main value of the threading operation is its usefulness as a building block for Markov chain Monte Carlo methods for sampling from an approximate posterior distribution over ARGs given the data. We employ three main types of sampling algorithms based on threading, as described below.

**Sequential sampling.** First, the threading operation can be applied iteratively to a series of orthologous sequences to obtain an ARG of size  $n$  from sequence data alone. This method works by randomly choosing one sequence and constructing for it a trivial ARG  $G^1$  (i.e. every local tree is a single branch). Additional sequences are then threaded into the ARG, one at a time, until an ARG  $G^n$  of  $n$  sequences has been obtained. Notice that an ARG derived in this manner is not a valid sample from the posterior distribution, because each successive  $G^k$  (for  $k \in \{2, \dots, n-1\}$ ) is sampled conditional on only  $D^{1:k}$  (the first  $k$  sequences). Nevertheless, the sequential sampling algorithm is an efficient heuristic method for obtaining an initial ARG, which can subsequently be improved by other methods. If desired, this operation can be applied multiple times, possibly with various permutations of the sequences, to obtain multiple initializations of an MCMC sampler. Heuristic methods can also be used to choose a “smart” initial ordering of sequences. For example, one might begin with one representative of each of several human populations, to first approximate the overall ARG structure, and subsequently add more representatives of each population.

**Gibbs sampling for single sequences.** Second, the threading operation can serve as the basis of a Gibbs sampler for full ARGs. Starting with an initial ARG of  $n$  sequences, individual sequences can be removed, randomly or in round-robin fashion, and rethreaded. Since the threading procedure samples from the conditional distribution  $P(G^n | G^{n-1}, D^n, \Theta)$ , this produces a valid Gibbs sampler for the ARG up to the assumptions of the DSMC. The ergodicity of the Markov chain follows, essentially, from the fact that any tree is reachable from any other by a finite sequence of branch removals and additions (see Supplementary Methods for details).

The main limitation of this method is that it leads to poor mixing when the number of sequences grows large. The essential problem is that rethreading a single sequence is equivalent to resampling the placement of external branches in the local trees, so this method is highly inefficient at rearranging the “deep structure” (internal branches) of the ARG. Furthermore, this mixing problem becomes progressively worse as  $n$  grows. As a result, an alternative strategy is needed for large numbers of sequences.



**Subtree sampling.** The third sampling strategy addresses the mixing limitations of the Gibbs sampler by generalizing the threading operation to accommodate not only individual sequences but subtrees with arbitrary numbers of leaves. As a result, internal branches in the local trees can be resampled and the deep structure of the ARG can be perturbed. The subtree threading problem is considerably more difficult than the single-sequence threading problem, because, in general, the subtrees change in composition and structure along the sequence. In principle, one could arbitrarily select a subtree for each nonrecombining segment and resample its attachment point to the remainder of the tree, but because the attachment points at both ends of a segment would be constrained by the flanking local trees, there would be a strong tendency to resample the original attachment points, resulting in poor mixing of the sampler. Instead, we use an approach that allows us to select a sequence of subtrees guaranteed to have good continuity properties in order to enable long-range rethreading of internal branches. To select these sequences of subtrees, we use a data structure called a *branch graph*, which traces the parent/child relationships among branches across genomic positions. Using dynamic programming, it is possible to identify paths through the branch graph that correspond to sequences of internal branches with good continuity properties, resulting in efficient sampling of subtree threadings (see Supplementary Methods for details).

More specifically, after a sequence of internal branches is identified, the selected branch is removed from each local tree, splitting it into a main tree and a subtree. A new branch is then added above the root of every subtree and allowed to re-coalesce with the corresponding main tree in a manner consistent with the DSMC. As with the single-sequence threading operation, it is possible to sample directly from the desired conditional distribution under the DSMC. However, since the number of ways of removing internal branches depends on the current structure of the ARG, the Hastings ratio is not equal to one in this case, and a more general Metropolis-Hastings algorithm (with rejection of some proposed threadings) is required (see Supplementary Methods for details). In practice, the acceptance rates for proposed threadings are fairly high ( $\sim 40\%$  for typical human data) and this strategy substantially improves the mixing properties of the Gibbs sampler. This generalized sampling strategy allows the number of sequences to be increased substantially (see below).

## ***ARGweaver* Program**

We implemented these sampling strategies in a computer program called *ARGweaver*, that “weaves” together an ARG by repeated applications of the threading operation. The program has subroutines for threading of both individual sequences and subtrees. Options allow it to be run as a Gibbs sampler with single-sequence threading or a general Metropolis-Hastings sampler with subtree threading. In either case, sequential sampling is used to obtain an initial ARG. Arguments to the program specify the number of sampling iterations and the frequency with which samples are recorded. The program is written in C++ and is reasonably well optimized. For example, it requires about 1 second to sample a threading of a single 1 Mb sequence in an ARG of 20 sequences with 20 time steps. Our source code is available upon request.

To summarize and visualize samples from the posterior distribution over ARGs, we used two main strategies. First, we summarized the sampled ARGs in terms of three statistics per genomic position: the time to most recent common

ancestor (TMRCA), recombination rate, and a statistic we call “local effective population size” (local  $N_e$ ), which is essentially a measure of inverse coalescence rate in genealogies in the region (see Methods). In some cases, we also considered the estimated age of the derived alleles at polymorphic sites, which we obtain by mapping the mutation to a branch in the local tree and calculating the average time for that branch. We computed posterior mean and 95% credible intervals for each of these statistics per genomic position, and created genome browser tracks to allow these values to be visualized together with other types of annotation along the human genome.

Second, we explored multi-dimensional visualization schemes that would expose more of the rich complexity of the ARG, yet still be intuitive and interpretable at multiple genomic scales. After some experimentation, we settled on a representation we call a “leaf trace.” A leaf trace contains a line for genome sequence in an analyzed data set. At each genomic position, these nodes are ordered according to the local genealogy for that position, and the spacing between adjacent lines is proportional to the time to their most recent common ancestor (Figure 4A). These lines extend along the genome, proceeding in parallel in nonrecombining segments, then crossing and/or becoming closer or farther apart where recombinations occur. Notice that a leaf trace represents a single ARG, rather than a distribution of possible ARGs. We use the single most likely ARG sampled by *ARGweaver* as the basis for our plots. Several features of interest are immediately evident from a leaf trace. For example, recombination hot spots show up as regions with dense clusters of line crossings, whereas recombination cold spots are indicated by long blocks of parallel lines (Figure 4B).

## Simulation Study

### Evaluation of Discretized Sequentially Markov Coalescent in Data Generation

Before turning to inference, we examine the effects of time discretization on various properties of interest in simulated data sets. Following McVean and Cardin [37], we compared data sets generated under the DSMC with ones generated under the sequentially Markov coalescent (SMC) and the coalescent-with-recombination (CwR). First, we simulated 1 Mb regions of 20 sequences, assuming reasonable values for  $N$  and  $\mu$  for human populations and a plausible range of recombination rates (data set #1, Table 1). We carried out parallel simulations under the DSMC, the SMC, and the CwR, assuming various numbers of time intervals ( $K$ ) for the DSMC. At all recombination rates, the DSMC, SMC, and CwR models produced very similar distributions of recombination counts (Supplementary Figure S1A). These distributions were essentially indistinguishable at lower recombination rates, and the DSMC exhibited only a slight excess of recombinations events at higher rates. Interestingly, the DSMC appeared not to be highly sensitive to the number of time intervals  $K$ , although the excess in recombination events at high rates was most pronounced under the most coarse-grained discretization scheme ( $K = 10$ ).

In a second simulation experiment, we assumed a single recombination rate and considered four effective population sizes ( $N$ ), ranging from 2,500 to 10,000 individuals (data set #2, Table 1). In this comparison, we used the number of segregating sites as the summary statistic of interest. As expected, this statistic increases approximately linearly with  $N$  under all models. Once again, we found that the CwR, SMC, and DSMC models produced nearly identical

distributions of counts, with only a minor inflation under the coarsest discretization schemes (Supplementary Figure S1B). These simulated data sets could be additionally be compared in terms of decay of linkage disequilibrium, but it is unlikely that the discretization assumed in the DSMC would significantly degrade the performance of the SMC by this measure [37]. Overall, these comparisons indicate that the discretization scheme used by the DSMC has at most a minimal effect on measurable patterns of mutation and recombination at realistic parameter values for human populations, suggesting that the model will be adequate for use in inference.

### Convergence of Sampler

We next evaluated the convergence properties of the MCMC sampler on simulated data. With small numbers of sequences, the Gibbs sampler based on the single-sequence threading operation appeared to converge rapidly, according to both the complete data log likelihood for the sampled ARG and the sequences, and the inferred numbers of recombination events. (Notice that the complete data log likelihood—the logarithm of equation 16—is a measure that captures both recombination and mutation events.) However, when the number of sequences grew larger than about 6–8 (depending on the specific details of the simulation), the Gibbs sampling strategy was no longer adequate. The subtree threading operation and the general Metropolis-Hastings sampler appear to address this problem effectively, allowing the number of sequences to be pushed to 20 or more (Supplementary Figure S2). With 20 sequences 1 Mb in length, the sampler converges to true values within about 500 sampling iterations, which takes about 20 minutes on a desktop computer.

### Recovery of Global ARG Features

In our next series of experiments, we systematically assessed the ability of *ARGweaver* to recover several features of interest from simulated ARGs over a range of plausible ratios of mutation to recombination rates (data set #3, Table 1). In this experiment, we considered three “global” features of the ARG: (i) the total number of recombinations, (ii) the complete data log likelihood (log of equation 16), and (iii) the total branch length of the ARG. We define the total branch length to be the sum of the total branch lengths of the local trees at all sites, a quantity proportional to the expected number of mutations in the history of the sample, and, if the population-scaled mutation rate is low (as it is here), one approximately proportional to the expected number of segregating sites. We applied *ARGweaver* to each data set with 200 burn-in iterations, followed by 1000 sampling iterations, with every tenth sample retained (100 samples total).

We found that *ARGweaver* was able to recover the features of interest fairly accurately at most parameter settings (Figure 5). The estimates of the log likelihood and number of recombinations appeared to be unbiased for all values of  $\mu/\rho$ . In addition, the variance in these estimates was generally low, especially at higher values of  $\mu/\rho$ . The total branch length of the ARG was also well estimated for  $\mu/\rho \geq 4$ , but it exhibited a slight downward bias at  $\mu/\rho = 2$  and a more pronounced downward bias at  $\mu/\rho = 1$ . These are the scenarios in which the signal for the local trees is weakest, and the bias toward lower total branch lengths appears to come from the prior distribution. Notably, most current estimates of average rates would place the true ratio of mutation to recombination rates for human populations

between 1 and 2 [56–58], suggesting that we may expect some bias in branch lengths with real data. However, the concentration of human recombination events in hot spots implies that the ratio should be considerably more favorable for our methods across most of the genome. In any case, the bias from a low  $\mu/\rho$  ratio appears to be modest and to have a limited influence on other quantities, such as the inferred number of recombinations.

### Recovery of Local ARG Features

An advantage of explicitly sampling full ARGs is that it enables inferences about local features of the ARG that are not directly determined by model parameters (see also [27]). Using the simulated data and inference procedure as in the previous section, we evaluated the performance of *ARGweaver* in estimating three representative quantities along the genome sequence: (i) time to most recent common ancestry (TMRCA), (ii) recombination rate, and (iii) allele age. We estimated each quantity using an approximate posterior expected value, computed by averaging across sampled ARGs. The TMRCA was computed directly per genomic position, while the recombination rate was computed in a sliding window of 1 kb. The mutation age was computed only at polymorphic sites. With 20 sequences, we found that *ARGweaver* was able to recover the TMRCA with remarkably high accuracy and high resolution (Figure 6). The accuracy of TMRCA inference degrades somewhat for lower values of the ratio  $\mu/\rho$  but remains quite good even with  $\mu/\rho = 1$  (data not shown). To study recombination rates, we generated simulated data by a slightly modified procedure, allowing for intermittent recombination hot spots designed to mirror those in real human sequences. We found that power was weak with only 20 sequences, but with 100 sequences the reconstructed ARGs clearly displayed elevated rates of recombination in the hotspots compared with the flanking regions (Supplementary Figure S3). Estimates of allele ages appeared to be unbiased, with reasonable concordance between true and estimated values, although the variance in the estimates was fairly high (Supplementary Figure S4). Together, these results suggest that, even with modest numbers of sequences, the distributions of ARGs inferred by our methods may be informative about loci under natural selection, local recombination rates, and other local features of evolutionary history.

### Accuracy of Local Tree Topologies

In our next experiment, we evaluated the accuracy of *ARGweaver* in inferring the topology of the local trees. The local trees are a more complex feature of the ARG but are of particular interest for applications such as genotype imputation and association mapping. We applied the method to simulated data set #3 (Table 1), running the MCMC sampler each time for 1000 iterations (200 burn-in). For comparison, we also inferred local trees using the only other available ARG reconstruction method that can be readily applied on this scale, the heuristic *Margarita* program [34]. To compare the two programs, we identified 100 evenly spaced locations in the simulated data sets, and extracted the local trees reconstructed by both methods at these positions. We compared the trees inferred by *ARGweaver* and *Margarita* with the true local trees generated during simulation by two measures of topological similarity: branch correctness (one minus the normalized Robinson-Foulds (RF) distance [59]) and Maximum Agreement Subtree (MAST) percentage (the size of the largest leaf-set such that induced subtrees are topologically equivalent, expressed as a percentage of the total number of leaves). We found that, for all mutation and recombination rates tested, *ARGweaver* produced

significantly more accurate local tree topologies than *Margarita* by each of these metrics (Supplementary Figure S5). The improvements were most pronounced at high  $\mu/\rho$  ratios (where topological information is greatest) but were evident across all ratios considered. They were also most pronounced when measured by MAST percentage, which is less sensitive to minor differences between trees than the branch-wise measure. Notably, the absolute accuracy of the trees inferred by *ARGweaver* was fairly high, given the sparseness of informative sites in these data sets. For example, at  $\mu/\rho = 6$ , more than four of five predicted branches were correct and MAST percentages approached 75%, and even in the challenging case of  $\mu/\rho = 1$ , roughly two of three branches were correct and MAST percentages exceeded 50%. These results indicate that the sampler is effectively pooling information from many sites across the multiple alignment in making inferences about the local trees.

### Accuracy of Branch Uncertainty

In principle, a fully Bayesian method for ARG inference should provide not only accurate estimates of ARG features of interest, but also a useful measurement of the uncertainty associated with those features. To evaluate the performance of *ARGweaver* in measuring uncertainty of this kind, we grouped individual branches into bins according to their estimated posterior probabilities (i.e., the fraction of sampled local trees in which each branch is found), and compared these values with the relative frequencies with which the same branches were observed in the true trees. We found that the predicted and actual probabilities of correctness were closely correlated, indicating that *ARGweaver* is accurately measuring the uncertainty associated with the local trees (Supplementary Figure S6). By contrast, the heuristic *Margarita* sampler shows a clear tendency to overestimate the confidence associated with branches in the local trees, often by 10–20%. This comparison is not entirely fair, because the authors of *Margarita* do not claim that it samples from the posterior distribution, but it nevertheless highlights a major advantage of the Bayesian approach. The ability to accurately measure uncertainty in features of the ARG has many potential benefits, including improved accuracy of posterior expected values that depend on highly uncertain aspects of the ARG (such as mutation age estimates) and improved tests of statistical significance.

### Analysis of Real Data

Having demonstrated that *ARGweaver* was able to recover many features of simulated ARGs with reasonable accuracy, we turned to a preliminary analysis of real human genome sequences. For this analysis we chose to focus on sequences for 54 unrelated individuals from the “69 genomes” data set from Complete Genomics (<http://www.completegenomics.com/public-data/69-Genomes>) [60]. This data set is well suited for an initial analysis with *ARGweaver* because (i) the sequences are of high coverage and high quality, minimizing any potential impact from genotyping error; (ii) they include representation from multiple, diverse human populations; and (iii) the number of sequences is of a scale that can be accommodated with our current implementation.

The 54 genome sequences were computationally phased and were filtered in various ways to minimize the influence from genotype and alignment errors. They were partitioned into 2 Mb blocks and *ARGweaver* was applied to these blocks in parallel on a computer cluster. For this analysis, we assumed  $K = 20$ ,  $s_K = 1,000,000$  generations, and  $N =$

21,739 (corresponding to  $\theta = 4N\mu = 0.001$  and  $\mu = 1.2 \times 10^{-8}$ ), and we allowed for variation across loci in mutation and recombination rates. For each 2 Mb block, we collected samples for 2,000 iterations of the sampler, after a 200 iteration burn-in (see Methods for details).

### General Features of Inferred ARG

We began by summarizing the sampled ARGs using genome browser tracks for TMRCA, local  $N_e$ , and recombination rate, as described above. When compared with other genomic annotations, these summary statistics showed several expected patterns, suggesting that they are capturing true properties of the evolutionary history of the analyzed sequences. For example, the inferred recombination rates generally exhibit prominent peaks at known recombination hot spots, more so than can be explained by the use of the HapMap recombination map in the prior (Supplementary Figure S7). The TMRCA and local  $N_e$  measures are variable at individual loci, but when they are averaged across many loci a clear dependency on proximity to genic elements can be observed, evidently due to the effects of selection at linked sites (Figure 7). Not only are both TMRCA and local  $N_e$  significantly reduced in the neighborhood of genes, showing fairly steep declines over 10–20 kilobases upstream and downstream of genes, but they also exhibit U-shaped patterns across the gene bodies themselves, probably because the cumulative effect of selection from linked sites is greatest near the middle of gene bodies. Similarly, extremely low TMRCA ( $<20,000$  generations) are significantly enriched in annotation types known to be under strong selection, such as coding sequences (CDS) and untranslated regions (UTRs) of known genes, but depleted in regions that tend not to be strongly influenced by selection, such as repeats and intergenic regions (Table 2). It is worth noting that the local  $N_e$  statistic is closely related to measures of background selection, such as the statistic  $B$  recently computed genome-wide by McVicker et al. [61]. However, both TMRCA and local  $N_e$  could be influenced by hitchhiking as well as by background selection.

We also examined leaf traces for several loci of interest. In addition to identifying recombination hot spots, we found that these diagrams were effective in highlighting the conserved haplotype structure around regions known to have been influenced by selective sweeps, such as the lactase promoter region (Figure 4C). We found that it was particularly informative to “anchor” the diagram at a particular locus by coloring the plot in a canonical order (such as a rainbow spectrum) at that locus, and then observe the manner in which the haplotype structure decays around it. Work is in progress to build genome-browser tracks based on the leaf-trace paradigm. We also plan to continue to experiment with alternative visualization approaches that capture complementary aspects of the inferred distribution of ARGs (see Discussion).

### Inference of Population Network

More work will be needed to develop our ARG-sampling methods into a full framework for demography inference, similar to coalescent-based methods that apply to small numbers of sequences [18, 39, 41, 42] or ignore intralocus recombination [62–64] (see Discussion). Nevertheless, even when a demographically naive prior distribution is assumed (based on a single panmictic population of fixed size), we expect samples drawn from the posterior distribution of ARGs to contain useful information about demographic history. To explore the usefulness of our current imple-

mentation of *ARGweaver* in characterizing population structure, we extracted local trees from our sampled ARGs and analyzed them with methods that attempt to infer a species or population network from a collection of (possibly discordant) gene trees based on parsimony criteria.

We began by considering eight populations that have been suggested by other studies to exhibit relatively low levels of admixture: the Yoruba (YRI), Luhya (LWK), Maasai (MKK), Tuscan (TSI), Utah residence of Northern and Western European ancestry from the Centre d’Etude de Polymorphisme Humain collection (CEU), Indian (GIH), Han Chinese (CHB), and Japanese (JPT) populations. We extracted several hundred local trees from our sampled ARGs and reduced each tree to the subtree in which only these seven populations were represented, then analyzed the trees with the PhyloNet package. In this case, we used the MDC algorithm of Than and Nakhleh [65], which finds a population tree that minimizes the number of “deep coalescences” required for reconciliation with a given set of gene trees. This method is appropriate here because discordances between gene trees and the population phylogeny are expected to result primarily from incomplete lineage sorting (see, e.g., [66]). The MDC algorithm did indeed produce a tree consistent with the accepted phylogeny for these populations, with the deepest divergence event between African and Eurasian populations, and successively more recent events separating the European from the Asian populations, the West African Yoruba from the East African Luhya and Maasai, and the South Asian Indian population from the East Asian Han Chinese and Japanese. The most recent events separated the relatively geographically and ethnically similar Tuscan and CEU populations, Luhya and Massai populations, and Han Chinese and Japanese populations (Figure 8A).

Next we examined a more difficult case, in which the heavily admixed African American population was included in place of the Indian population. We continued to use the PhyloNet program to analyze the gene trees in which these populations were represented, but in this case, we used an extension of the MDC algorithm that infers a phylogenetic network that allows for hybridization between species or populations along with incomplete lineage sorting [67]. Using this algorithm, PhyloNet reconstructed a network similar to the expected version, but with some distortion among the Tuscan, Maasai, and African American populations (Figure 8B). The program correctly identified the presence of admixture in this part of the network, but had difficulty with the direction of gene flow, treating the Maasai as a genetic mixture of unobserved sister populations of the African Americans and Tuscans, rather than identifying the African Americans as the most admixed group, as expected. This apparent error results from some unknown combination of various possible causes, including error and/or uncertainty in gene tree inference and inadequacies of the model for hybridization or the parsimony-based objective function. Additional work will be needed to see whether these limitations can be addressed, and to compare inferences based on post-processing of samples from *ARGweaver* with direct inference of a full parametric demographic model (see Discussion). Nevertheless, these experiments suggest that the posterior distribution of ARGs does contain useful information about population structure even when an uninformative prior distribution is used.

## Discussion

While the general statistical characteristics of population samples of genetic markers in the presence of recombination have been apparent for decades [21, 68–71], solutions to the problem of explicitly characterizing this structure in the general case of multiple markers and multiple sequences—that is, of making direct inferences about the ancestral recombination graph (ARG) [19, 20]—have been elusive. Recent investigations have led to important progress on this problem based on the Sequentially Markov Coalescent (SMC) [18, 37–42], but existing methods are still either restricted to small numbers of sequences or require heavy approximations. In this paper, we introduce a method that is faithful to the SMC yet has much better scaling properties than previous methods. These properties depend on a novel “threading” operation that can be performed in a highly efficient manner using hidden Markov modeling techniques. Inference does require the use of Markov chain Monte Carlo (MCMC) sampling, which has certain costs, but we have shown that the sampler mixes fairly well and converges rapidly, particularly if it is augmented with operations that simultaneously thread multiple sequences. For the first time, our methods allow explicit statistical inference of ARGs on the scale of complete mammalian genomes. In addition, the sampling of ARGs from their posterior distribution—while costly in some respects—has the important advantage of allowing estimation of the distribution of any ARG-derived quantity, such as times to most recent common ancestry, recombination rates, or regions of identity by descent.

Our methods are similar in some respects to the conditional sampling distribution (CSD)-based methods of Song and colleagues [50–53], despite that we have arrived at them by a different route. In particular, both approaches consider a conditional distribution for the  $n$ th sequence given the previous  $n - 1$  sequences, and in both cases, a discretized SMC is exploited for efficiency of inference. However, there is a crucial difference between the two strategies: the CSD-based methods consider the marginal distribution of the  $n$ th sequence only, given the other  $n - 1$  sequences, while ours considers the joint distribution of an ARG of size  $n$  and the  $n$  sequence, given an ARG of size  $n - 1$  and the previous  $n - 1$  sequences. In this sense, we have employed a “data augmentation” strategy, explicitly representing full ARGs in order to simplify intermediate calculations with consideration of full genealogies. The cost of this strategy is that it requires Markov chain Monte Carlo methods for inference, rather than allowing direct likelihood calculations and maximum-likelihood parameter estimation. The benefit is that it provides an approximate posterior distribution over complete ARGs and derived quantities, including times to most recent common ancestry, distributions of coalescence times, gene flow between populations, and similar quantities. By contrast, the CSD-based methods provide information about only those properties of the ARG that are directly described by the model parameters. We view these two approaches as complementary and expect that, in many cases, they will be best suited for somewhat different types of analyses.

We believe that our ARG sampling framework has the potential for broad applicability in statistical population genomics. As a proof of concept, we have shown that our methods can recover TMRCAs and recombination rates from both simulated and real data, and that features such as the TMRCA and local  $N_e$  show the expected patterns around elements under selection. We have also shown that the sampled ARGs contain useful information about population structure, although more work is needed to properly accommodate admixed populations. In addition, our approach



could be useful for a wide variety of other applications, including local ancestry inference [48, 72, 73], haplotype phasing / genotype imputation [47, 49, 74, 75], association/LD mapping [76–81], and the detection of natural selection [82–85]. It may also be possible to use our methods to make progress on the difficult problem of distinguishing background selection and hitchhiking [61, 86, 87], which should give rise to distinct distributions of coalescence times. Additional work will be needed to identify the cases in which the advantages of methods that make use of explicit representations of ARGs are sufficient to offset their computational cost.

Demography inference is an application area of particular interest in the recent literature [17, 18, 52, 53, 88]. By generalizing the PSMC approach [42] to multiple genomes, our approach has the potential to allow not only improved estimation of ancestral population sizes over a broader range of time scales, but also to allow direct inference of population divergence times and migration rates for multiple populations simultaneously. In this way it can be seen as a potential means for generalizing Bayesian coalescent-based methods for demography inference, such as MCMC-coal [62, 63] and G-PhoCS [64], to a setting in which recombination is allowed and complete genome sequences are considered. Importantly, the use of the complete ARG would allow information about demographic history from both patterns of mutation and patterns of linkage disequilibrium to be naturally integrated (see discussion in [64]). However, as with CSD-based methods [52, 53], an extension to a full, parametric multi-population model for application on a genome-wide scale would be technically challenging. In our case, it would require the ability to sample “threadings” consistent with the constraints of a population model (e.g., with no coalescent events between genetically isolated populations) and exploration of a full collection of population parameters. Because Bayesian coalescent-based methods that ignore recombination already require long running times, an extension to full ARGs will be difficult, but we believe it can be achieved for at least moderate numbers of genomes through careful optimization of the sampler. An alternative approach would be to sample ARGs under a model that assumes a panmictic population (as we use now) and then to perform demographic inference in a post-processing step based on the sampled genealogies, as in our initial attempts at estimating population phylogenies. This approach would depend on the data being sufficiently informative to drive the inference procedure, despite the use of a noninformative prior. One interesting possibility along these lines would be to use the sampled genealogies as a proposal distribution for an inference method that uses importance sampling or MCMC to estimate a full demographic model. By decoupling the ARG sampling and demography inference steps, this approach might improve on the efficiency and scalability of methods that simultaneously infer ARGs and multi-population demographic models.

We have used a number of approximations to simplify our methods, with apparently minimal impact on performance with (real or simulated) human sequence data. Nevertheless, some of these simplifications may no longer be appropriate in other applications. For example, following Li and Durbin [42], we compute probabilities of recombination between discrete genomic positions under the assumptions of the continuous-space SMC [37]. When recombination rates are low, the discrete and continuous models are nearly identical, but the differences between them can become significant when recombination rates are higher (A. Hobolth and J. L. Jensen, “Markovian approximation to the finite loci coalescent with recombination along multiple sequences,” submitted.). Similarly, our assumption of at most one recombination event per site and our use of the SMC rather than the improved SMC’ [38] may lead to

biases in cases of higher recombination rates, larger numbers of sequences, or more divergent sequences. The use of the SMC' may be particularly important in accurately accounting for historical recombination events over longer evolutionary time periods, where we expect many “diamond” or “bubble” recombinations (i.e., recombinations followed immediately by coalescences of the recombining lineage, going backward in time; this is the additional class of events considered by the SMC'). In addition, our heuristic approach of accommodating zero-length branches by randomly sampling among “active” branches for coalescence and recombination events (see Methods) is not strictly justified by the principles underlying the DSMC, and may lead to biases when the discretization scheme is coarse relative to the frequencies of the events of interest. It is possible to accommodate more precise solutions to all of these issues within our general framework, and some extensions (such as the use of the SMC' or Hobolth and Jensen's transition density) would be fairly trivial, but others (such as allowing for multiple recombinations per site across the full ARG) would require more work. It will be important in future research to weigh the costs of possible extensions against their potential benefits with an eye toward particular applications of interest.

Another limitation of our current methods is that, as currently implemented, they require haploid genome sequences as input. In most cases of current interest, diploid organisms have been sequenced with short-read technologies, and heterozygous positions must be computationally phased before the data can be analyzed. Errors in phasing, if they occur at appreciable rates, are likely to produce biases in our inference procedure. In particular, we expect some over-estimation of recombination and mutation rates in the presence of phasing error, because the sampler will compensate for phasing errors with additional recombination and/or mutation events. An ideal solution for this problem would be to enable the method to work directly with unphased data and integrate over all possible phasings (see, e.g., [64, 89]). It appears to be possible to adapt the threading operation to integrate over phasings on the forward pass then sample a particular phase in backward pass, as we currently do with recombinations. In principle, this approach should allow simultaneous threading and phasing, not only enabling the analysis of unphased data but also producing a set of phased sequences as a by-product of the analysis. This approach could also be extended to allow imputation of missing genotypes. More needs to be done to demonstrate that this approach is feasible but it appears to be a promising avenue for future work.

The ability to perform explicit ARG inference on the scale of complete genomes opens up a wide range of possible applications, but the long running times required for these analyses and the unwieldy data structures they produce (numerous samples of ARGs) may be barriers to practical usefulness. One strategy for addressing this problem would be to precompute ARGs for data sets of particular interest and provide publicly available tools for data retrieval and visualization. For example, one could carefully analyze a particularly rich public data set, such as the high-coverage genome sequences currently being produced by the 1000 Genomes Project [90], and extract a modest number of samples (say, 1000) from a lengthy MCMC run. These samples could be stored in a database in a manner that allowed researchers to efficiently extract various features of interest, such as marginal genealogies, recombination events, regions of IBD, or times to most recent common ancestry. In this way, a single ARG sampling run could be used to enable a broad variety of downstream analyses. A related possibility would be to support on-the-fly “threading” of user-specified query sequences into precomputed ARGs. This operation would be analogous to local ancestry

inference [48,72,73], but would reveal not only the population sources of query sequence segments, but also additional information about recombination events, coalescence times, approximate mutation ages, and other features. The same operation could be used to allow our sampling methods to scale to thousands of genomes: one could infer ARGs for, say, 100 genomes, then simply thread in hundreds more, without full MCMC sampling. Finally, precomputed ARG samples could also be used as the basis for various visualization tracks, perhaps including the tracks like the ones introduced in this paper, as well as complementary tracks describe features of the ARG such as population divergence times, migration rates, or mutation ages. In general, posterior samples of ARGs will be a rich resource for the interpretation of genetic data, but it will be critical to find efficient and effective ways to make these samples practically useful to the genomics community.

## Methods

### Discretized Sequentially Markov Coalescent

#### Discretization Scheme and Notation

The Discretized Sequentially Markov Coalescent (DSMC) assumes that all coalescence and recombination events occur at  $K + 1$  discrete time points,  $\mathcal{P} = \{s_0, s_1, s_2, \dots, s_K\}$ , with  $s_0 = 0$  (the present time) and  $s_K$  equal to a user-specified maximum value. These time points are defined in units of generations before the present time. We evenly distribute these time points on a logarithmic scale, so that the discretization scheme has finer resolution near the leaves of the ARG, where more events are expected to occur. Specifically, we define  $s_j$  (for  $0 \leq j \leq K$ ) to be  $s_j = g(j)$ , where

$$g(j) = \frac{1}{\delta} \left\{ \exp \left[ \frac{j}{K} \log(1 + \delta s_K) \right] - 1 \right\}. \quad (3)$$

Here,  $s_K$  is the maximum time and  $\delta$  is a tuning parameter that, when increased, causes the time points to become more densely clustered near the leaves of the ARG. Notice that  $g(0) = 0$  and  $g(K) = s_K$ . In this work, we have assumed  $s_K = 200,000$  generations and  $\delta = 10$ . We denote the length of time interval  $j$  as  $\Delta s_j = s_{j+1} - s_j$ . The DSMC process is defined such that it approaches the continuous SMC as a limit as  $K \rightarrow \infty$  and each  $\Delta s_j \rightarrow 0$ , with  $s_K$  sufficiently large that the probability of a coalescence event older than  $s_K$  is close to zero.

It is useful to specify “midpoints” between time points (on a log scale), to facilitate rounding of continuous-valued times to the nearest discrete time point. We define the midpoint between times  $s_j$  and  $s_{j+1}$  (for  $0 \leq j < K$ ) as  $s_{j+\frac{1}{2}} = g(j + \frac{1}{2})$ . We can alternatively refer to the midpoint between times  $s_{j-1}$  and  $s_j$  as  $s_{j-\frac{1}{2}} = g(j - \frac{1}{2})$  (for  $1 \leq j \leq K$ ), noting that  $s_{j-\frac{1}{2}} = g(j - \frac{1}{2}) = g((j-1) + \frac{1}{2}) = s_{(j-1)+\frac{1}{2}}$ . Coalescence events that occur between  $s_{j-\frac{1}{2}}$  and  $s_{j+\frac{1}{2}}$  are “rounded” to time point  $s_j$ . We found that it was less critical to round recombination events to the nearest time point, so they are simply rounded to the next most recent time point (see below). We denote the lengths of the half intervals between  $j - \frac{1}{2}$  and  $j$ , and between  $j$  and  $j + \frac{1}{2}$ , as  $\Delta s_{j-\frac{1}{2},j}$  and  $\Delta s_{j,j+\frac{1}{2}}$ , respectively.

Because all coalescence events must occur at the designated time points, the collection of branches is fixed for each interval  $j$  between time points  $s_j$  and  $s_{j+1}$ . Given a local tree  $T_i^n$  that is consistent with the DSMC, we denote the

set of branches in time interval  $j$  as  $B(T_i^n, j)$ . The size of this set,  $|B(T_i^n, j)|$ , is of particular interest, and is abbreviated  $B_j$  (with  $T_i^n$  clear from context). In addition, it is often of interest to consider the branch sets for a tree  $T_i^n$  from which a branch  $w$  has been removed. We denote such a tree by  $T_i^{n,(-w)}$  and abbreviate the number of branches in interval  $j$  as  $B_j^{(-w)}$  (again, with  $T_i^n$  clear from context).

One consequence of discretizing time is that the DMSC will tend to generate ARGs that contain many branches of length zero (corresponding to polytomies in the local trees), which will have zero probability of recombination, coalesce, or mutation events. In effect, the rounding procedure will tend to shrink short branches to zero, which may lead to distortions in data generation and inference. We address this problem heuristically, by defining the DSMC to first sample the times of recombination and coalescence events, and then randomly select a branch from all of those “active” at the sampled time point. We define the set of active branches at a time point  $s_j$ , for a local tree  $T_i^n$ , to be those branches in  $T_i^n$  that start, end, or pass through  $s_j$ . This set is denoted  $A(T_i, j)$  and its size is abbreviated as  $A_j$ . As above, we use  $A_j^{(-w)}$  to indicate the active branches at  $s_j$  excluding branch  $w$ . Simulations indicate that this heuristic solution to the problem of zero-length branches works fairly well in practice (see Figure S1).

### Recombination Process

As in the standard SMC, recombinations are assumed to occur according to a Poisson process with rate  $\rho|T_{i-1}^n|$ , where  $|T_{i-1}^n|$  is the total branch length of local tree  $T_{i-1}^n$  and  $\rho$  is the average number of recombinations/generation/site. Once a recombination occurs, the ordinary SMC process places the recombination uniformly along the branches of  $T_{i-1}^n$ . The analogous operation of sampling a recombination branch and time point,  $R_i^n = (w, s_k)$ , in the DSMC is accomplished by first sampling a time point  $s_k$  in proportion to the total branch length present during time interval  $k$ , then randomly selecting one of the  $A_k$  branches active at that time point. Consistent with the assumptions of the SMC, the recombination point cannot occur above the time point associated with the root  $r$  of tree  $T_{i-1}^n$ , which we denote  $s_r$ . Thus, the sampling distribution for a recombination point  $R_i^n$  on a local tree  $T_{i-1}^n$  is given by,

$$P(R_i^n | T_{i-1}^n, \Theta) = \begin{cases} \exp(-\rho|T_{i-1}^n|) & \text{if } R_i^n = \emptyset \\ \frac{1}{A_k} \cdot \frac{B_k \Delta s_k}{C} \cdot [1 - \exp(-\rho|T_{i-1}^n|)] & \text{if } R_i^n = (w, s_k), w \in A(T_{i-1}^n, k), 0 \leq s_k < s_r \\ \frac{1}{2} \cdot \frac{\Delta s_k}{C} \cdot [1 - \exp(-\rho|T_{i-1}^n|)] & \text{if } R_i^n = (w, s_k), w \in A(T_{i-1}^n, r) \setminus \{r\}, s_k = s_r \\ 0 & \text{otherwise,} \end{cases} \quad (4)$$

where  $C = \sum_{j=0}^r B_j \Delta s_j$  is a constant that explicitly normalizes the distribution over time points  $s_0, \dots, s_r$ . The special case for the time point at the root of the tree,  $s_k = s_r$ , is required because the SMC does not allow recombinations to occur beyond this point, so the effective number of active branches is only two at this time point, despite that  $A_r$  will have a value of three. The number of branches in the interval above the root,  $B_r$ , is necessarily one, so this term can be omitted in this case.

This sampling distribution effectively rounds the times of recombination events downward to the next most recent time point. However, a strict policy of downward rounding, together with a prohibition against recombination events

above the root node, would make it impossible to sample recombination events at time point  $s_r$ , which turns out to have undesirable effects in inference (it makes some trees unreachable by the threading operation). Therefore, when sampling time points, we use the heuristic approach of imagining that recombinations can also occur in the time interval immediately above the root and assigning these events to the time point  $s_r$ . This has the effect of redistributing some of the probability mass from later time points to the root, without altering the overall rate at which recombinations occur ( $\rho|T_{i-1}^n|$ ). For this reason, the normalizing constant  $C$  differs slightly from the total branch length  $|T_{i-1}^n|$ ; in particular,  $C = |T_{i-1}^n| + \Delta s_r$ . It would be slightly more elegant to allow upward as well as downward rounding of times for recombinations, as we do with coalescence events (see below), but as long as the time discretization is not too coarse these differences are of minor importance, and the approach we have used seems to be adequate.

### Re-coalescence Process

Once a recombination point  $R_i^n = (w, s_k)$  is sampled, the selected branch  $w$  is removed from time points  $s_k$  and older, and allowed to re-coalesce to the remainder of the tree, in a manner analogous to the SMC. Because we explicitly prohibit multiple recombinations between adjacent positions, the local tree  $T_i^n$  must be reachable from  $T_{i-1}^n$  by a single “subtree pruning and regrafting” (SPR) operation corresponding to the recombination, i.e., an operation that cuts a branch of the tree at the recombination point and re-attaches it (and any descendant nodes) to the remainder of the tree. Thus, we can write,

$$P(T_i^n | R_i^n, T_{i-1}^n, \Theta) = \begin{cases} 1 & \text{if } R_i^n = \emptyset, T_i^n = T_{i-1}^n \\ P(x, s_j | w, s_k, T_{i-1}^n, \Theta) & \text{if } R_i^n = (w, s_k), (x, s_j) \text{ s.t. } T_i^n = \text{SPR}(T_{i-1}^n, w, s_k, x, s_j), s_j \geq s_k \\ 0 & \text{otherwise,} \end{cases} \quad (5)$$

where  $\text{SPR}(T_{i-1}^n, w, s_k, x, s_j)$  is a function that returns the new tree produced by an SPR operation on  $T_{i-1}^n$  that cuts branch  $w$  at time  $s_k$  and re-attaches it to branch  $x$  at time  $s_j$ , and  $P(x, s_j | w, s_k, T_{i-1}^n, \Theta)$  is a joint conditional distribution over re-coalescence branches and time points.

The main challenge is therefore to define the discrete re-coalescence distribution,  $P(x, s_j | w, s_k, T_{i-1}^n, \Theta)$ , for  $s_j \geq s_k$  (as required by the SMC). There are two distinct cases to consider:  $s_j > s_k$  and  $s_j = s_k$ . When  $s_j > s_k$ , the unattached branch  $w$  must first fail to re-coalesce during the interval between  $s_k$  and  $s_{j-\frac{1}{2}}$ , and then must re-coalesce between  $s_{j-\frac{1}{2}}$  and  $s_{j+\frac{1}{2}}$  (because all such re-coalescence events will be rounded to  $s_j$ ). By contrast, when  $s_j = s_k$ , the branch  $w$  must simply re-coalesce between  $s_j (= s_k)$  and  $s_{j+\frac{1}{2}}$  (because the re-coalescence time is strictly bounded by the recombination time).

In all cases, the instantaneous rate of re-coalescence in each interval  $l$  ( $k \leq l \leq j$ ) is given by  $B_l^{(-w)}/(2N_l)$ , in the standard manner for the coalescent. (Note that we use  $B_l^{(-w)}$  rather than  $B_l$ , because we are concerned with the coalescence rate to the remainder of the tree, excluding branch  $w$ . We also assume a diploid species throughout, so the total number of chromosomes per locus is  $2N$ .) The probability that a lineage starting at a time  $s_l$  coalesces before

$s_{l+1}$  is given by the cumulative distribution function for exponentially distributed waiting times,

$$W(l, l+1) = 1 - \exp\left(-\frac{B_l^{(-w)} \Delta s_l}{2N_l}\right), \quad (6)$$

and the probability of coalescence during a sequences of intervals,  $m, m+1, \dots, n-1$  is given by,

$$W(m, n) = 1 - \exp\left(-\sum_{l=m}^{n-1} \frac{B_l^{(-w)} \Delta s_l}{2N_l}\right). \quad (7)$$

Similarly, the probabilities of coalescence during the half intervals before and after time point  $s_l$  are given, respectively, by,

$$W\left(l - \frac{1}{2}, l\right) = 1 - \exp\left(-\frac{B_{l-1}^{(-w)} \Delta s_{l-\frac{1}{2}, l}}{2N_{l-1}}\right), \quad W\left(l, l + \frac{1}{2}\right) = 1 - \exp\left(-\frac{B_l^{(-w)} \Delta s_{l, l+\frac{1}{2}}}{2N_l}\right). \quad (8)$$

Thus, the distribution of re-coalescence times for the case of  $s_j > s_k$  is given by,

$$\begin{aligned} P(s_j | w, s_k, T_{i-1}^n, \Theta) &= \left[1 - W\left(k, j - \frac{1}{2}\right)\right] \times W\left(j - \frac{1}{2}, j + \frac{1}{2}\right) \\ &= \exp\left[-\left(\sum_{l=k}^{j-2} \frac{B_l^{(-w)} \Delta s_l}{2N_l}\right) - \frac{B_{j-1}^{(-w)} \Delta s_{j-1, j-\frac{1}{2}}}{2N_{j-1}}\right] \times \left[1 - \exp\left(-\frac{B_{j-1}^{(-w)} \Delta s_{j-\frac{1}{2}, j}}{2N_{j-1}} - \frac{B_j^{(-w)} \Delta s_{j, j+\frac{1}{2}}}{2N_j}\right)\right]. \end{aligned} \quad (9)$$

The probability of re-coalescence for the case of  $s_j = s_k$  is simply,

$$P(s_j = s_k | w, s_k, T_{i-1}^n, \Theta) = W\left(k, k + \frac{1}{2}\right) = \left[1 - \exp\left(-\frac{B_k^{(-w)} \Delta s_{k, k+\frac{1}{2}}}{2N_k}\right)\right]. \quad (10)$$

Finally, the requirement for re-coalescence by the maximum time,  $s_K$ , is enforced by explicitly normalizing the distribution:

$$P(s_j = s_K | w, s_k, T_{i-1}^n, \Theta) = 1 - \sum_{l=k}^{K-1} P(s_l | w, s_k, T_{i-1}^n, \Theta). \quad (11)$$

Once the coalescence time point  $s_j$  is chosen, a lineage  $x$  is uniformly chosen from the  $A_j^{(-w)}$  active lineages in  $T_i$  at that time point, similar to the process for recombination events. Thus,  $P(x, s_j | w, s_k, T_{i-1}^n, \Theta) = \frac{1}{A_j^{(-w)}} P(s_j | w, s_k, T_{i-1}^n, \Theta)$ , and equation 5 can be rewritten as,

$$P(T_i^n | R_i^n, T_{i-1}^n, \Theta) = \begin{cases} 1 & \text{if } R_i^n = \emptyset, T_i^n = T_{i-1}^n \\ \frac{1}{A_j^{(-w)}} P(s_j | w, s_k, T_{i-1}^n, \Theta) & \text{if } R_i^n = (w, s_k), (x, s_j) \text{ s.t. } T_i^n = \text{SPR}(T_{i-1}^n, w, s_k, x, s_j), s_k \leq s_j \leq s_K \\ 0 & \text{otherwise,} \end{cases} \quad (12)$$

where  $P(s_j | w, s_k, T_{i-1}^n, \Theta)$  is given by equations 9–11.

## Initial Local Tree

The DSMC begins by generating an initial local tree,  $T_1^n$ , using a discretized version of the coalescent process. This process can be decomposed into two steps: (1) the generation of a sequence of branch counts,  $\mathbf{C} = (C_0, C_1, \dots, C_K)$  for time points  $s_0, s_1, \dots, s_K$ , and (2) sampling of a topology  $\mathcal{T}_1^n$  consistent with these branch counts. The probability of an observed initial tree  $T_1^n$  can therefore be calculated as,

$$P(T_1^n | \Theta) = P(\mathcal{T}_1^n, \mathbf{C} | \Theta) = P(\mathbf{C} | \mathbf{N}) P(\mathcal{T}_1^n | \mathbf{C}), \quad (13)$$

where  $\mathbf{N}$  is a vector of effective population sizes,  $\mathbf{N} = (N_0, \dots, N_K)$ . The branch count for time 0 is constrained to be equal to the number of samples,  $C_0 = n$ , and the branch count for time  $K$  is required to be one,  $C_K = 1$  (see below).

Since the coalescent process is Markovian in time, the distribution for the vector of branch counts can be factored by time intervals,

$$P(\mathbf{C} | \mathbf{N}) = P(C_0) \prod_{l=1}^K P(C_l | C_{l-1}, \Delta s_{l-1}, N_{l-1}), \quad (14)$$

with degenerate first and last terms,  $P(C_0) = I[C_0 = n]$  and  $P(C_K | C_{K-1}, N_{K-1}) = I[C_K = 1]$ .

The conditional distributions of the form  $P(C_l | C_{l-1}, \Delta s_{l-1}, N_{l-1})$ , for  $1 \leq l < K$ , have been derived previously as [91],

$$P(C_l = b | C_{l-1} = a, \Delta s_{l-1} = t, N_{l-1}) = \sum_{k=b}^a \exp\left(\frac{-k(k-1)}{4N_{l-1}}t\right) \frac{(2k-1)(-1)^{k-b}}{b!(k-b)!(k+b-1)} \prod_{y=0}^{k-1} \frac{(b+y)(a-y)}{a+y}. \quad (15)$$

## Hidden Markov Model

### Hidden Markov Model for Full Threading Problem

Let us first consider the complete data likelihood function under the DSMC, that is, the probability of an ARG  $\mathbf{G}^n = (\mathbf{T}^n, \mathbf{R}^n)$  and a sequence alignment  $\mathbf{D}^n$  given the model parameters. In our notation, this function is given by,

$$P(\mathbf{T}^n, \mathbf{R}^n, \mathbf{D}^n | \Theta) = P(T_1^n | N) P(D_1^n | T_1^n, \mu) \prod_{i=2}^L P(R_i^n | T_{i-1}^n, \rho) P(T_i^n | R_i^n, T_{i-1}^n, N) P(D_i^n | T_i^n, \mu). \quad (16)$$

If the full ARG  $\mathbf{G}^n = (\mathbf{T}^n, \mathbf{R}^n)$  is regarded as a latent variable, this equation defines a hidden Markov model with a state space given by all possible pairs  $(T_i^n, R_i^n)$ , transition probabilities given by expressions of the form  $P(R_i^n | T_{i-1}^n, \rho)$   $P(T_i^n | R_i^n, T_{i-1}^n, N)$  and emission probabilities given by  $P(D_i^n | T_i^n, \mu)$  (see Figure 3A). The transition probabilities can be computed using equations 4 and 12, and the emission probabilities can be computed using Felsenstein's pruning algorithm. Indeed, the model can be viewed as an instance of the "phylo-HMMs" that have been widely used in comparative genomics [92]. However, as discussed in the Results section, unless the number of sequences  $n$  is very small, the state space of this HMM will be too large to allow it to be used directly for inference.

Instead, we constrain the inference problem by fixing the ARG for the first  $n-1$  sequences,  $\mathbf{G}^{n-1}$ , and sampling

from the conditional distribution  $P(\mathbf{G}^n \mid \mathbf{G}^{n-1}, \mathbf{D}, \Theta)$ . Using the notation  $\mathbf{G}^n = (\mathbf{T}^n, \mathbf{R}^n)$  and  $\mathbf{G}^{n-1} = (\mathbf{T}^{n-1}, \mathbf{R}^{n-1})$ , we define  $\mathbf{T}^n = (\mathbf{T}^{n-1}, \mathbf{Y})$ , where  $\mathbf{Y} = (y_1, \dots, y_L)$  is a vector of coalescence points such that  $y_i = (x_i, t_i)$  indicates a coalescence of the  $n$ th sequence to branch  $x_i$  and time point  $y_i$  of local tree  $T_i^{n-1}$ , and  $\mathbf{R}^n = (\mathbf{R}^{n-1}, \mathbf{Z})$ , where  $\mathbf{Z} = (z_2, \dots, z_L)$  is a vector of recombination points such that  $z_i = (w_i, u_i)$  indicates a recombination at branch  $w_i$  and time point  $u_i$  of local tree  $T_{i-1}^{n-1}$  between positions  $i-1$  and  $i$ . (Note that  $z_1$  is undefined.) Thus, we can sample from the desired conditional distribution  $P(\mathbf{G}^n \mid \mathbf{G}^{n-1}, \mathbf{D}, \Theta)$  by sampling from  $P(\mathbf{Y}, \mathbf{Z} \mid \mathbf{T}^{n-1}, \mathbf{R}^{n-1}, \mathbf{D}^n, \Theta)$ . We refer to a sample  $(\mathbf{Y}, \mathbf{Z})$  from this distribution as a *threading* of the  $n$ th sequence through the ARG (see Figure 3B).

Note that the restriction to one recombination event per position implies that  $z_i = \emptyset$  wherever  $R_i^{n-1} \neq \emptyset$ , and that  $T_{i-1}^{n-1} = T_i^{n-1}$  wherever  $z_i \neq \emptyset$ . This restriction is not strictly required but it simplifies the description of new recombination events  $z_i$  and, in the setting in which we are interested, it comes with little cost (see Discussion).

It turns out to be more convenient to work with the joint distribution  $P(\mathbf{T}^{n-1}, \mathbf{Y}, \mathbf{R}^{n-1}, \mathbf{Z}, \mathbf{D}^n \mid \Theta)$  (the complete data likelihood) than with the conditional distribution  $P(\mathbf{Y}, \mathbf{Z} \mid \mathbf{T}^{n-1}, \mathbf{R}^{n-1}, \mathbf{D}^n, \Theta)$ . However, to emphasize that the variables  $\mathbf{T}^{n-1}$  and  $\mathbf{R}^{n-1}$  are held fixed (“clamped”) at pre-specified values throughout the threading operation, we denote them as  $\bar{\mathbf{T}}^{n-1}$  and  $\bar{\mathbf{R}}^{n-1}$ , and refer to the distribution of interest as  $P(\bar{\mathbf{T}}^{n-1}, \mathbf{Y}, \bar{\mathbf{R}}^{n-1}, \mathbf{Z}, \bar{\mathbf{D}}^n \mid \Theta)$ . (Notice that the data  $\mathbf{D}^n$  are also clamped, as usual for HMMs.) When  $\mathbf{T}^{n-1}$ ,  $\mathbf{R}^{n-1}$ , and  $\mathbf{D}^n$  are clamped,

$$P(\bar{\mathbf{T}}^{n-1}, \mathbf{Y}, \bar{\mathbf{R}}^{n-1}, \mathbf{Z}, \bar{\mathbf{D}}^n \mid \Theta) \propto P(\mathbf{Y}, \mathbf{Z} \mid \bar{\mathbf{T}}^{n-1}, \bar{\mathbf{R}}^{n-1}, \bar{\mathbf{D}}^n, \Theta). \quad (17)$$

Thus, samples of  $(\mathbf{Y}, \mathbf{Z})$  drawn in proportion to the unnormalized density  $P(\bar{\mathbf{T}}^{n-1}, \mathbf{Y}, \bar{\mathbf{R}}^{n-1}, \mathbf{Z}, \bar{\mathbf{D}}^n \mid \Theta)$  will be valid samples from the desired conditional distribution.

We can now write the density function for the (unnormalized) sampling distribution for a threading  $(\mathbf{Y}, \mathbf{Z})$  as,

$$\begin{aligned} P(\bar{\mathbf{T}}^{n-1}, \mathbf{Y}, \bar{\mathbf{R}}^{n-1}, \mathbf{Z}, \bar{\mathbf{D}}^n \mid \Theta) = \\ P(\bar{\mathbf{T}}_1^{n-1}, y_1 \mid N) P(\bar{\mathbf{D}}_1 \mid \bar{\mathbf{T}}_1^{n-1}, y_1, \mu) \prod_{i=2}^L P(\bar{\mathbf{R}}_i^{n-1}, z_i \mid \bar{\mathbf{T}}_{i-1}^{n-1}, y_{i-1}, \rho) P(\bar{\mathbf{T}}_i^{n-1}, y_i \mid \bar{\mathbf{R}}_i^{n-1}, z_i, \bar{\mathbf{T}}_{i-1}^{n-1}, y_{i-1}, N) \\ \times P(\bar{\mathbf{D}}_i \mid \bar{\mathbf{T}}_i^{n-1}, y_i, \mu), \end{aligned} \quad (18)$$

where all terms are computable using previously described expressions, as for equation 16.

Notice that this threading HMM has the same conditional independence structure as the HMM for the full DSMC (equation 16, Figure 3), but its state space is now defined by sets of possible  $(y_i, z_i)$  pairs rather than the set of possible  $(T_i^n, R_i^n)$  pairs, making it far more tractable for inference.

### Reduced Model for Coalescent Threading

The state space can be reduced further by proceeding in two steps. First, we sample a *coalescent threading*  $\mathbf{Y}$  from the marginal distribution  $P(\bar{\mathbf{T}}^{n-1}, \mathbf{Y}, \bar{\mathbf{R}}^{n-1}, \bar{\mathbf{D}}^n \mid \Theta) \propto P(\mathbf{Y} \mid \bar{\mathbf{T}}^{n-1}, \bar{\mathbf{R}}^{n-1}, \bar{\mathbf{D}}^n, \Theta)$ . Then we sample a *recombination threading*,  $\mathbf{Z}$ , from the conditional distribution  $P(\mathbf{Z} \mid \mathbf{Y}, \bar{\mathbf{T}}^{n-1}, \bar{\mathbf{R}}^{n-1}, \Theta)$ . Notice that the data need not be considered when sampling the recombination threading, because  $\mathbf{Z}$  is conditionally independent of  $\mathbf{D}^n$  given  $\mathbf{Y}$ ,  $\mathbf{T}^{n-1}$ , and  $\mathbf{R}^{n-1}$ .



The marginal distribution  $P(\bar{T}^{n-1}, Y, \bar{R}^{n-1}, \bar{D}^n | \Theta)$  can be computed efficiently by changing the order of products and sums in the usual way for HMMs (e.g., [93]):

$$\begin{aligned}
P(\bar{T}^{n-1}, Y, \bar{R}^{n-1}, \bar{D}^n | \Theta) &= \sum_Z P(\bar{T}^{n-1}, Y, \bar{R}^{n-1}, Z, \bar{D}^n | \Theta) \\
&= P(\bar{T}_1^{n-1}, y_1 | N) P(\bar{D}_1 | \bar{T}_1^{n-1}, y_1, \mu) \prod_{i=2}^L \left[ \sum_{z_i} P(\bar{R}_i^{n-1}, z_i | \bar{T}_{i-1}^{n-1}, y_{i-1}, \rho) P(\bar{T}_i^{n-1}, y_i | \bar{R}_i^{n-1}, z_i, \bar{T}_{i-1}^{n-1}, y_{i-1}, N) \right] \\
&\quad \times P(\bar{D}_i | \bar{T}_i^{n-1}, y_i, \mu) \\
&= P(\bar{T}_1^{n-1}, y_1 | N) P(\bar{D}_1 | \bar{T}_1^{n-1}, y_1, \mu) \prod_{i=2}^L P(\bar{R}_i^{n-1}, \bar{T}_i^{n-1}, y_i | \bar{T}_{i-1}^{n-1}, y_{i-1}, \rho, N) P(\bar{D}_i | \bar{T}_i^{n-1}, y_i, \mu). \tag{19}
\end{aligned}$$

This equation defines an HMM with a state space given by the possible values of  $y_i$  only, the size of which is bounded by  $nK$ , where  $n$  is the number of sequences and  $K$  is the number of time intervals (see Figure 3C).

While this model has the conditional independence structure of a standard HMM, the state space is heterogeneous along the sequence, because the set of possible coalescent points at each position  $i$  depends on the local tree,  $\bar{T}_i^{n-1}$ . (The full threading HMM described above also has this property.) If we denote the state space at position  $i$  as  $S_i$ , the transition probabilities between states in position  $i$  and states in position  $i+1$  are defined by a  $|S_i| \times |S_{i+1}|$  transition matrix  $A_i = \{a_{l,m}^i\}$  where  $l$  and  $m$  index the states of  $|S_i|$  and  $|S_{i+1}|$ , respectively, and  $a_{l,m}^i$  can be computed as,

$$\begin{aligned}
a_{l,m}^i &= P(\bar{R}_{i+1}^{n-1}, \bar{T}_{i+1}^{n-1}, y_{i+1} = m | \bar{T}_i^{n-1}, y_i = l, \rho, N) \\
&= \sum_{z_{i+1}} P(\bar{R}_{i+1}^{n-1}, z_{i+1} | \bar{T}_i^{n-1}, y_i = l, \rho) P(\bar{T}_{i+1}^{n-1}, y_{i+1} = m | \bar{R}_{i+1}^{n-1}, z_{i+1}, \bar{T}_i^{n-1}, y_i = l, N) \tag{20}
\end{aligned}$$

using equations 4 and 12. The emission probability for alignment column  $D_i^n$  in state  $l$  in  $S_i$  is denoted  $b_l^i(D_i^n) = P(D_i | \bar{T}_i^{n-1}, y_i = l, \mu)$  and can be computed using Felsenstein's pruning algorithm, as in all cases above. The initial state probabilities for the HMM are given by  $\pi_l = P(\bar{T}_1^{n-1}, y_1 = l | N)$  for  $1 \leq l \leq |S_1|$  and can be computed using equations 13–15.

Notice that, unlike with a standard, locally normalized HMM, it is not true in this model that  $\sum_m a_{l,m}^i = 1$ . Furthermore, for two positions  $i$  and  $j$ , it is not true in general that  $\sum_m a_{l,m}^i = \sum_m a_{l,m}^j$ , because of differences across positions in the local trees  $\bar{T}_i^{n-1}$  and recombination points  $\bar{R}_i^{n-1}$ . Similarly, it is not true that the sum of the emission probabilities  $b_l^i(D_i^n)$  over all possible values of  $D_i^n$  (all alignment columns of size  $n$ ) is equal to one, nor that this sum must be the same at any two positions  $i$  and  $j$ . Finally, it is not true that  $\sum_l \pi_l = 1$ . Thus, this model is not only globally unnormalized, but it also has a heterogeneous local normalization structure across positions. It is these unusual features of the threading HMM that make it more convenient to work with the clamped joint distribution than with the conditional distributions of direct interest.

## Stochastic Traceback

Despite the unusual features of the HMM described in the previous section, it still permits the use of standard dynamic programming algorithms to integrate over all coalescent threadings  $\mathbf{Y}$  (the forward or backward algorithms), obtain a most likely threadings  $\hat{\mathbf{Y}}$  (the Viterbi algorithm), compute marginal posterior distributions for each  $y_i$  (forward-backward algorithm), and sample threadings in proportion to their conditional probability [94, 95]. These algorithms depend only on the linear conditional independence structure of the model (and, equivalently, on its factorization into local transition and emission probabilities) and on the use of nonnegative potential functions, both properties that are maintained in this model.

We are primarily interested in a dynamic programming algorithm for sampling from the posterior distribution over HMM paths that is sometimes referred to as the *stochastic traceback* algorithm [95–97]. In our case, each application of this algorithm is guaranteed to sample a coalescent threading  $\mathbf{Y}$  in proportion to the density  $P(\bar{\mathbf{T}}^{n-1}, \mathbf{Y}, \bar{\mathbf{R}}^{n-1}, \bar{\mathbf{D}}^n | \Theta)$ , and equivalently, in proportion to the desired conditional distribution.

The stochastic traceback algorithm consists of a deterministic forward pass and a stochastic backward pass. The forward pass is identical to the forward algorithm. In our notation, the algorithm recursively fills out a matrix  $\mathbf{F} = \{f_{i,m}\}$ ,  $1 \leq i \leq L$ ,  $1 \leq m \leq \max_i(|\mathcal{S}_i|)$ . Each  $f_{i,m}$  represents the probability of a prefix of the data joint with a constraint on the state path at position  $i$ . Here,  $f_{i,m} = P(\bar{\mathbf{T}}_{1:i}^{n-1}, \bar{\mathbf{R}}_{1:i}^{n-1}, \bar{\mathbf{D}}_{1:i}, y_i = m | \Theta)$ , where the notation  $\mathbf{X}_{i:j}$  indicates the subsequence  $(X_i, \dots, X_j)$ . After an initialization of  $f_{1,m} = \pi_m b_m^1(D_1^n)$ , for  $1 \leq m \leq |\mathcal{S}_1|$ , the algorithm proceeds iteratively for  $i$  from 2 to  $L$  and sets each value  $f_{i,m}$  (for  $1 \leq l \leq |\mathcal{S}_i|$ ) equal to,

$$f_{i,m} = b_m^i(D_i^{n-1}) \sum_{l=1}^{|\mathcal{S}_{i-1}|} f_{i-1,l} a_{l,m}^{i-1}. \quad (21)$$

Note that the heterogeneity of the state space along the sequence implies that portions of the matrix are left undefined.

In the backward pass, the algorithm samples a sequence  $\mathbf{Y}$  one element at a time, starting with  $y_L$  and working backward to  $y_1$ . First,  $y_L = l$  is simply sampled in proportion to  $f_{L,l}$ . Then, for  $i$  from  $L-1$  down to 1, each  $y_i$  is sampled conditional on  $y_{i+1}$  in proportion to,

$$q_i(y_i = l | y_{i+1} = m) \propto f_{i,l} a_{l,m}^i. \quad (22)$$

The limiting step of the algorithm is the forward pass, which in general requires  $O(C^2L)$  time, where  $C$  is the size of the state space. However, in our case the sparsity of the  $\mathbf{A}_i$  matrices can be exploited to reduce the running time to  $O(nK^2L)$  (see Supplementary Methods).

It can be shown by induction on suffixes of  $\mathbf{Y}$  that this procedure will correctly sample from the target distribution,  $P(\mathbf{Y} | \bar{\mathbf{T}}^{n-1}, \bar{\mathbf{R}}^{n-1}, \bar{\mathbf{D}}^n, \Theta)$ . Briefly, in the base case, the suffix  $y_L = l$  is by construction sampled from the density  $f_{L,l} = P(\bar{\mathbf{T}}^{n-1}, \bar{\mathbf{R}}^{n-1}, \bar{\mathbf{D}}^n, y_L = l | \Theta)$ , which is proportional to the desired conditional distribution,  $P(y_L = l | \bar{\mathbf{T}}^{n-1}, \bar{\mathbf{R}}^{n-1}, \bar{\mathbf{D}}^n, \Theta)$ . For the inductive case, assume  $\mathbf{Y}_{i+1:L}$  has been sampled from  $P(\mathbf{Y}_{i+1:L} | \bar{\mathbf{T}}^{n-1}, \bar{\mathbf{R}}^{n-1}, \bar{\mathbf{D}}^n, \Theta)$ .

The procedure of sampling  $y_i$  from  $q_i$  given  $y_{i+1}$  is equivalent to sampling from,

$$\begin{aligned} q_i(y_i = l \mid y_{i+1} = m) &\propto f_{i,l} a_{l,m}^i = P(\bar{\mathbf{T}}_{1:i}^{n-1}, \bar{\mathbf{R}}_{1:i}^{n-1}, \bar{\mathbf{D}}_{1:i}^n, y_i = l \mid \Theta) P(\bar{\mathbf{R}}_{i+1}^{n-1}, \bar{\mathbf{T}}_{i+1}^{n-1}, y_{i+1} = m \mid \bar{\mathbf{T}}_i^{n-1}, y_i = l, \rho, N) \\ &= P(\bar{\mathbf{T}}_{1:i+1}^{n-1}, \bar{\mathbf{R}}_{1:i+1}^{n-1}, \bar{\mathbf{D}}_{1:i}^n, y_i = l, y_{i+1} = m \mid \Theta) \\ &\propto P(y_i = l \mid \mathbf{Y}_{i+1:L}, \bar{\mathbf{T}}^{n-1}, \bar{\mathbf{R}}^{n-1}, \bar{\mathbf{D}}^n, \Theta), \end{aligned} \quad (23)$$

where the last step is possible because  $y_i$  is conditionally independent of  $\mathbf{Y}_{i+2:L}$ ,  $\mathbf{T}_{i+2:L}^n$ ,  $\mathbf{R}_{i+2,L}^n$ , and  $\mathbf{D}_{i+1:L}^n$  given  $y_{i+1}$ . Thus, the algorithm will correctly sample from  $P(\mathbf{Y}_{i:L} \mid \bar{\mathbf{T}}^{n-1}, \bar{\mathbf{R}}^{n-1}, \bar{\mathbf{D}}^n, \Theta)$  for all  $i$  such that  $1 \leq i \leq L$ .

### Sampling a Recombination Threading

The final step in the threading operation is to sample a recombination threading  $\mathbf{Z}$  conditional on a coalescent threading  $\mathbf{Y}$  and the clamped parameters. This step is greatly simplified by the fact that the individual  $z_i$  values are conditionally independent of one another given the  $y_i$  variables and the clamped  $\mathbf{T}_i^{n-1}$  and  $\mathbf{R}_i^{n-1}$  variables (see Figure 3B). Consequently, each  $z_i$  can be sampled separately from the distribution,

$$P(z_i \mid \bar{\mathbf{R}}_i^{n-1}, \bar{\mathbf{T}}_i^{n-1}, \bar{y}_i, \bar{\mathbf{T}}_{i-1}^{n-1}, \bar{y}_{i-1}, \Theta) \propto P(\bar{\mathbf{R}}_i^{n-1}, z_i \mid \bar{\mathbf{T}}_{i-1}^{n-1}, \bar{y}_{i-1}, \rho) P(\bar{\mathbf{T}}_i^{n-1}, \bar{y}_i \mid \bar{\mathbf{R}}_i^{n-1}, z_i, \bar{\mathbf{T}}_{i-1}^{n-1}, \bar{y}_{i-1}, N), \quad (24)$$

where the  $y_i$  variables are now clamped along with the  $\mathbf{T}_i^{n-1}$  and  $\mathbf{R}_i^{n-1}$  variables. Notice that the distribution on the RHS is the same one considered in equations 19 & 20. The normalizing constant for this distribution, for clamped values  $\bar{y}_{i-1} = l$  and  $\bar{y}_i = m$ , is given by the transition probability  $a_{l,m}^{i-1}$ .

Notice that this distribution is implicitly degenerate in the case in which  $\bar{\mathbf{R}}_i^{n-1} \neq \emptyset$ , owing to the limitation of at most one recombination event per position. In particular, if  $\bar{\mathbf{R}}_i^{n-1} \neq \emptyset$ , then  $P(\bar{\mathbf{R}}_i^{n-1}, z_i \mid \bar{\mathbf{T}}_{i-1}^{n-1}, \bar{y}_{i-1}, \rho) = I[z_i = \emptyset]$ , hence  $P(z_i \mid \bar{\mathbf{R}}_i^{n-1}, \bar{\mathbf{T}}_i^{n-1}, \bar{y}_i, \bar{\mathbf{T}}_{i-1}^{n-1}, \bar{y}_{i-1}, \Theta) = I[z_i = \emptyset]$ . At the same time, notice that, if  $\bar{\mathbf{R}}_i^{n-1} = \emptyset$ , a new recombination is still possible ( $z_i \neq \emptyset$ ) even if  $\bar{\mathbf{T}}_{i-1}^{n-1} = \bar{\mathbf{T}}_i^{n-1}$  and  $\bar{y}_{i-1} = \bar{y}_i$ , because a branch could be broken by a recombination event but then re-coalesce at precisely its original position in the local tree.

The efficiency of sampling from this distribution can be improved by noting that most possible  $z_i$  values have zero probability, even when  $\bar{\mathbf{R}}_i^{n-1} \neq \emptyset$ . Let  $\mathcal{Z}$  represent the set of  $z_i$  values having nonzero probability for given values of  $y_{i-1}$ ,  $y_i$ , and  $v$ , where  $v$  denotes the branch being threaded. There are two cases to consider, a main case and a special case. We will denote the corresponding subsets of  $z_i$  values  $\mathcal{Z}_1$  and  $\mathcal{Z}_2$ , with  $\mathcal{Z} = \mathcal{Z}_1 \cup \mathcal{Z}_2$ . Recall that  $z_i = (w_i, u_i)$  and  $y_i = (x_i, t_i)$ , where  $x_i$  and  $w_i$  are branches in  $\mathbf{T}_{i-1}^{n-1}$  and  $\mathbf{T}_i^{n-1}$ , respectively, and  $u_i$  and  $t_i$  are time points from the set  $\mathcal{P} = \{s_0, \dots, s_K\}$ . In the main case, the recombination occurs on the new branch  $v$ . Here, the recombination time  $u_i$  must be at least as recent as both the old and new re-coalescence times,  $t_{i-1}$  and  $t_i$ . Thus,  $\mathcal{Z}_1 = \{(v, u_i) \mid u_i \in \mathcal{P}, u_i \leq \min(t_{i-1}, t_i)\}$ . Notice that  $|\mathcal{Z}_1| \leq K + 1$ .

The special case occurs when the recombination occurs not on the new branch,  $v$ , but instead on  $x_{i-1}$ , the branch to which  $v$  re-coalesces at position  $i - 1$ . A recombination on branch  $x_{i-1}$ , below the point at which  $v$  joins it, followed by a re-coalescence of  $x_{i-1}$  to  $v$  (meaning that  $x_i = x_{i-1}$ ) will produce a signature exactly like the symmetric case of

a recombination on  $v$  followed by a re-coalescence to  $x_{i-1}$  (Supplementary Figure S8), so this scenario must also be considered. This case can only occur when  $x_{i-1} = x_i$  and in the interval of time between the start of branch  $x_i$  and  $\min(t_{i-1}, t_i)$ . Hence,

$$Z_2 = \begin{cases} \{(x_i, u_i) \mid u_i \in \mathcal{P}, u_i \geq s_k, u_i \leq \min(t_{i-1}, t_i)\} & x_{i-1} = x_i \\ \emptyset & \text{otherwise,} \end{cases} \quad (25)$$

where  $s_k$  is the time point of the child node of branch  $x_i$ . As with  $Z_1$ ,  $|Z_2| \leq K + 1$ .

By enumerating the elements of  $Z$ , it is possible to sample each  $z_i$  in  $O(K)$  time. The same approach can be used to enable calculation of the  $a_{l,m}^i$  values (equation 20) in  $O(K)$  time.

## Data Preparation

### Simulated Data

Except where noted otherwise, simulations were performed under the full coalescent-with-recombination model [21]. Additional simulations (e.g., for Supplementary Figure S1) were performed under the Sequentially Markov Coalescent as described by McVean and Cardin [37], and under the Discretized Sequentially Markov Coalescent, as detailed in this article. In all cases, after generation of local trees, sequence alignments were generated using a finite-sites Jukes-Cantor model [54]. Parameter values for simulated data sets are summarized in Table 1. All simulations were performed using custom computer programs.

### Real Data

Information about human polymorphisms came from the “69 Genomes” data set from Complete Genomics (<http://www.completegenomics.com/public-data/69-Genomes/>). We considered 54 unrelated individuals from this set, excluding the child in each trio (YRI and PUR) and all but the four grandparents in the 17-member CEU pedigree. For each individual considered, we recorded the diploid genotype call reported for each position in the hg19 (Genome Reference Consortium Human Build 37) reference genome using CG’s ‘masterVar’ files. We considered both “SNPs” and “length-preserving substitutions” in the masterVar file. Borrowing from our previous work on demography inference [64], we applied several filters to these data to reduce the impact of technical errors from alignment, sequencing, genotype inference, and genome assembly. All positions that passed these filters and that were not annotated as polymorphic were assumed to be homozygous for the allele reported in the reference genome. Our analysis considered the autosomes only (chromosomes 1–22). The full set of 69 genomes was phased using Beagle 3.3.2 with the “lowmem” option on full chromosome sequences.

To sample ARGs genome-wide we split each sequence alignment into 2 Mb non-overlapping windows with 100 kb additional flanking sequence on either end. A core set of 12 individuals was chosen randomly such that each major population group was represented. We then used *ARGweaver* to sample ARGs for this core set of 24 haplotypes using a population size of  $N = 21739$ ,  $K = 20$  time steps, a maximum time of  $s_K = 1,000,000$  generations, and 2000 iterations with an initial burn-in of 200 iterations. In order to account for region-specific variation in recombination

and mutation rates, we used the HapMap phase II recombination map [98], and a mutation rate map estimated from alignments of several primate genomes, including chimpanzee (panTro2), orangutan (ponAbe2), and rhesus Macaque (rheMac2) [99]. Mutation rates were scaled to have an average of  $1.2 \times 10^{-8}$  mutations/generation/site and were averaged over 100kb non-overlapping windows.

## Supplementary Methods

A supplementary document providing details about the branch graph and subtree threading operation, calculation of the transition probabilities by dynamic programming, optimization of the forward algorithm, and related issues is available from the authors by request.

## Acknowledgments

This project was supported by a David and Lucile Packard Fellowship for Science and Engineering (to A.S.), NIH/NIGMS grant GM102192 (to A.S.), and a postdoctoral fellowship from the Cornell Center for Comparative and Population Genomics (to M.D.R.). We thank Ilan Gronau, Asger Hobolth, Thomas Mailund, Graham Coop, Richard Durbin, Gerton Lunter, Gil McVean, Bob Griffiths, and many others for helpful discussions.

## References

1. Hein J, Schierup M, Wiuf C (2005) *Gene genealogies, variation and evolution: a primer in coalescent theory*. Oxford University Press.
2. Wakeley J (2009) *Coalescent theory: an introduction*. Roberts & Co. Publishers.
3. Fisher RA (1930) *The Genetical Theory of Natural Selection*. Oxford University Press.
4. Wright S (1931) Evolution in Mendelian Populations. *Genetics* 16: 97–159.
5. Kimura M (1962) On the probability of fixation of mutant genes in a population. *Genetics* 47: 713–719.
6. Felsenstein J (1973) Maximum-likelihood and minimum-step methods for estimating evolutionary trees from data on discrete characters. *Syst Zool* 22: 240–249.
7. Felsenstein J (1981) Evolutionary trees from DNA sequences: a maximum likelihood approach. *J Mol Evol* 17: 368–376.
8. Menozzi P, Piazza A, Cavalli-Sforza L (1978) Synthetic maps of human gene frequencies in Europeans. *Science* 201: 786–792.
9. Kingman J (1982) The coalescent. *Stoch Process Appl* 13: 235–248.
10. Voight BF, Adams AM, Frisse LA, Qian Y, Hudson RR, et al. (2005) Interrogating multiple aspects of variation in a full resequencing data set to infer human population size changes. *Proc Natl Acad Sci USA* 102: 18508–18513.
11. Keightley PD, Eyre-Walker A (2007) Joint inference of the distribution of fitness effects of deleterious mutations and population demography based on nucleotide polymorphism frequencies. *Genetics* 177: 2251–2261.
12. Boyko AR, Williamson SH, Indap AR, Degenhardt JD, Hernandez RD, et al. (2008) Assessing the evolutionary impact of amino acid mutations in the human genome. *PLoS Genet* 4: e1000083.
13. Wall JD, Lohmueller KE, Plagnol V (2009) Detecting ancient admixture and estimating demographic parameters in multiple human populations. *Mol Biol Evol* 26: 1823–1827.
14. Gravel S, Henn BM, Gutenkunst RN, Indap AR, Marth GT, et al. (2011) Demographic history and rare allele sharing among human populations. *Proc Natl Acad Sci USA* 108: 11983–11988.
15. Lawson DJ, Hellenthal G, Myers S, Falush D (2012) Inference of population structure using dense haplotype data. *PLoS Genet* 8: e1002453.
16. Palamara PF, Lencz T, Darvasi A, Pe'er I (2012) Length distributions of identity by descent reveal fine-scale demographic history. *Am J Hum Genet* 91: 809–822.
17. Ralph P, Coop G (2013) The geography of recent genetic ancestry across Europe. *PLoS Biol* 11: e1001555.
18. Harris K, Nielsen R (2013) Inferring demographic history from a spectrum of shared haplotype lengths. *PLoS Genet* 9: e1003521.
19. Griffiths RC, Marjoram P (1996) Ancestral inference from samples of DNA sequences with recombination. *J Comput Biol* 3: 479–502.
20. Griffiths R, Marjoram P (1997) An ancestral recombination graph. In: Donnelly P, Tavaré S, editors, *Progress in Population Genetics and Human Evolution*, Springer Verlag. pp. 257–270.
21. Hudson RR (1983) Properties of a neutral allele model with intragenic recombination. *Theor Popul Biol* 23: 183–201.

22. Fearnhead P, Donnelly P (2001) Estimating recombination rates from population genetic data. *Genetics* 159: 1299–1318.
23. Griffiths RC, Marjoram P (1996) Ancestral inference from samples of DNA sequences with recombination. *J Comput Biol* 3: 479–502.
24. Kuhner MK, Yamato J, Felsenstein J (2000) Maximum likelihood estimation of recombination rates from population data. *Genetics* 156: 1393–1401.
25. Nielsen R (2000) Estimation of population parameters and recombination rates from single nucleotide polymorphisms. *Genetics* 154: 931–942.
26. Kuhner MK (2006) LAMARC 2.0: maximum likelihood and Bayesian estimation of population parameters. *Bioinformatics* 22: 768–770.
27. O’Fallon BD (2013) ACG: rapid inference of population history from recombining nucleotide sequences. *BMC Bioinformatics* 14: 40.
28. Hein J (1990) Reconstructing evolution of sequences subject to recombination using parsimony. *Math Biosci* 98: 185–200.
29. Hein J (1993) A heuristic method to reconstruct the history of sequences subject to recombination. *J Mol Evol* 36: 396–405.
30. Kececioglu J, Gusfield D (1998) Reconstructing a history of recombinations from a set of sequences. *Discrete Applied Mathematics* 88: 239–260.
31. Wang L, Zhang K, Zhang L (2001) Perfect phylogenetic networks with recombination. *J Comput Biol* 8: 69–78.
32. Song YS, Hein J (2005) Constructing minimal ancestral recombination graphs. *J Comput Biol* 12: 147–169.
33. Song YS, Wu Y, Gusfield D (2005) Efficient computation of close lower and upper bounds on the minimum number of recombinations in biological sequence evolution. *Bioinformatics* 21 Suppl 1: i413–422.
34. Minichiello MJ, Durbin R (2006) Mapping trait loci by use of inferred ancestral recombination graphs. *Am J Hum Genet* 79: 910–922.
35. Wu Y (2009) New methods for inference of local tree topologies with recombinant SNP sequences in populations. *IEEE/ACM Trans Comput Biol Bioinform* 8: 182–193.
36. Wiuf C, Hein J (1999) Recombination as a point process along sequences. *Theor Popul Biol* 55: 248–259.
37. McVean GAT, Cardin NJ (2005) Approximating the coalescent with recombination. *Philos Trans R Soc Lond B Biol Sci* 360: 1387–1393.
38. Marjoram P, Wall JD (2006) Fast “coalescent” simulation. *BMC Genet* 7: 16.
39. Hobolth A, Christensen OF, Mailund T, Schierup MH (2007) Genomic relationships and speciation times of human, chimpanzee, and gorilla inferred from a coalescent hidden markov model. *PLoS Genet* 3: e7.
40. Mailund T, Dutheil JY, Hobolth A, Lunter G, Schierup MH (2011) Estimating divergence time and ancestral effective population size of Bornean and Sumatran orangutan subspecies using a coalescent hidden Markov model. *PLoS Genet* 7: e1001319.
41. Mailund T, Halager AE, Westergaard M, Dutheil JY, Munch K, et al. (2012) A new isolation with migration model along complete genomes infers very different divergence processes among closely related great ape species. *PLoS Genet* 8: e1003125.
42. Li H, Durbin R (2011) Inference of human population history from individual whole-genome sequences. *Nature* 475: 493–496.

43. Li N, Stephens M (2003) Modeling linkage disequilibrium and identifying recombination hotspots using single-nucleotide polymorphism data. *Genetics* 165: 2213–2233.
44. Stephens M, Donnelly P (2000) Inference in molecular population genetics. *Journal of the Royal Statistical Society Series B (Statistical Methodology)* 62: pp. 605–655.
45. Stephens M, Scheet P (2005) Accounting for decay of linkage disequilibrium in haplotype inference and missing-data imputation. *Am J Hum Genet* 76: 449–462.
46. Marchini J, Howie B, Myers S, McVean G, Donnelly P (2007) A new multipoint method for genome-wide association studies by imputation of genotypes. *Nat Genet* 39: 906–913.
47. Howie BN, Donnelly P, Marchini J (2009) A flexible and accurate genotype imputation method for the next generation of genome-wide association studies. *PLoS Genet* 5: e1000529.
48. Price AL, Tandon A, Patterson N, Barnes KC, Rafaels N, et al. (2009) Sensitive detection of chromosomal segments of distinct ancestry in admixed populations. *PLoS Genet* 5: e1000519.
49. Li Y, Willer CJ, Ding J, Scheet P, Abecasis GR (2010) MaCH: using sequence and genotype data to estimate haplotypes and unobserved genotypes. *Genet Epidemiol* 34: 816–834.
50. Paul JS, Song YS (2010) A principled approach to deriving approximate conditional sampling distributions in population genetics models with recombination. *Genetics* 186: 321–338.
51. Paul JS, Steinrücken M, Song YS (2011) An accurate sequentially Markov conditional sampling distribution for the coalescent with recombination. *Genetics* 187: 1115–1128.
52. Sheehan S, Harris K, Song YS (2013) Estimating variable effective population sizes from multiple genomes: a sequentially Markov conditional sampling distribution approach. *Genetics* 194: 647–662.
53. Steinrücken M, Paul JS, Song YS (2013) A sequentially Markov conditional sampling distribution for structured populations with migration and recombination. *Theor Popul Biol* .
54. Jukes TH, Cantor CR (1969) Evolution of protein molecules. In: Munro H, editor, *Mammalian Protein Metabolism*, New York: Academic Press. pp. 21–132.
55. Husmeier D, Wright F (2001) Detection of recombination in DNA multiple alignments with hidden Markov models. *J Comput Biol* 8: 401–427.
56. Kong A, Gudbjartsson DF, Sainz J, Jonsdottir GM, Gudjonsson SA, et al. (2002) A high-resolution recombination map of the human genome. *Nat Genet* 31: 241–247.
57. Kong A, Frigge ML, Masson G, Besenbacher S, Sulem P, et al. (2012) Rate of de novo mutations and the importance of father's age to disease risk. *Nature* 488: 471–475.
58. Sun JX, Helgason A, Masson G, Ebenesersdottir SS, Li H, et al. (2012) A direct characterization of human mutation based on microsatellites. *Nat Genet* 44: 1161–1165.
59. Robinson DF, Foulds LR (1981) Comparison of phylogenetic trees. *Mathematical Biosciences* 53: 131–147.
60. Drmanac R, Sparks AB, Callow MJ, Halpern AL, Burns NL, et al. (2010) Human genome sequencing using unchained base reads on self-assembling dna nanoarrays. *Science* 327: 78–81.
61. McVicker G, Gordon D, Davis C, Green P (2009) Widespread genomic signatures of natural selection in hominid evolution. *PLoS Genet* 5: e1000471.
62. Rannala B, Yang Z (2003) Bayes estimation of species divergence times and ancestral population sizes using DNA sequences from multiple loci. *Genetics* 164: 1645–1656.
63. Burgess R, Yang Z (2008) Estimation of hominoid ancestral population sizes under bayesian coalescent models incorporating mutation rate variation and sequencing errors. *Mol Biol Evol* 25: 1979–1994.



64. Gronau I, Hubisz MJ, Gulko B, Danko CG, Siepel A (2011) Bayesian inference of ancient human demography from individual genome sequences. *Nature Genetics* 43: 1031–1034.
65. Than C, Nakhleh L (2009) Species tree inference by minimizing deep coalescences. *PLoS Comput Biol* 5: e1000501.
66. Siepel A (2009) Phylogenomics of primates and their ancestral populations. *Genome Res* 19: 1929–1941.
67. Yu Y, Barnett RM, Nakhleh L (2013) Parsimonious inference of hybridization in the presence of incomplete lineage sorting. *Syst Biol* .
68. Hill WG, Robertson A (1966) The effect of linkage on limits to artificial selection. *Genet Res* 8: 269–294.
69. Karlin S, McGregor J (1968) Rates and probabilities of fixation for two locus random mating finite populations without selection. *Genetics* 58: 141–159.
70. Strobeck C, Morgan K (1978) The effect of intragenic recombination on the number of alleles in a finite population. *Genetics* 88: 829–844.
71. Griffiths RC (1981) Neutral two-locus multiple allele models with recombination. *Theor Popul Biol* 19: 169–186.
72. Tang H, Coram M, Wang P, Zhu X, Risch N (2006) Reconstructing genetic ancestry blocks in admixed individuals. *Am J Hum Genet* 79: 1–12.
73. Sankararaman S, Sridhar S, Kimmel G, Halperin E (2008) Estimating local ancestry in admixed populations. *Am J Hum Genet* 82: 290–303.
74. Scheet P, Stephens M (2006) A fast and flexible statistical model for large-scale population genotype data: applications to inferring missing genotypes and haplotypic phase. *Am J Hum Genet* 78: 629–644.
75. Browning SR, Browning BL (2007) Rapid and accurate haplotype phasing and missing-data inference for whole-genome association studies by use of localized haplotype clustering. *Am J Hum Genet* 81: 1084–1097.
76. Rannala B, Reeve JP (2001) High-resolution multipoint linkage-disequilibrium mapping in the context of a human genome sequence. *Am J Hum Genet* 69: 159–178.
77. Larribe F, Lessard S, Schork NJ (2002) Gene mapping via the ancestral recombination graph. *Theor Popul Biol* 62: 215–229.
78. Zollner S, Pritchard JK (2005) Coalescent-based association mapping and fine mapping of complex trait loci. *Genetics* 169: 1071–1092.
79. Minichiello MJ, Durbin R (2006) Mapping trait loci by use of inferred ancestral recombination graphs. *Am J Hum Genet* 79: 910–922.
80. Wu Y (2008) Association mapping of complex diseases with ancestral recombination graphs: models and efficient algorithms. *J Comput Biol* 15: 667–684.
81. Besenbacher S, Mailund T, Schierup MH (2009) Local phylogeny mapping of quantitative traits: higher accuracy and better ranking than single-marker association in genomewide scans. *Genetics* 181: 747–753.
82. Voight BF, Kudaravalli S, Wen X, Pritchard JK (2006) A map of recent positive selection in the human genome. *PLoS Biol* 4: e72.
83. Sabeti PC, Varilly P, Fry B, Lohmueller J, Hostetter E, et al. (2007) Genome-wide detection and characterization of positive selection in human populations. *Nature* 449: 913–918.
84. Nielsen R, Williamson S, Kim Y, Hubisz MJ, Clark AG, et al. (2005) Genomic scans for selective sweeps using SNP data. *Genome Res* 15: 1566–1575.

85. Pickrell JK, Coop G, Novembre J, Kudaravalli S, Li JZ, et al. (2009) Signals of recent positive selection in a worldwide sample of human populations. *Genome Res* 19: 826–837.
86. Hellmann I, Mang Y, Gu Z, Li P, de la Vega FM, et al. (2008) Population genetic analysis of shotgun assemblies of genomic sequences from multiple individuals. *Genome Res* 18: 1020–1029.
87. Hernandez RD, Kelley JL, Elyashiv E, Melton SC, Auton A, et al. (2011) Classic selective sweeps were rare in recent human evolution. *Science* 331: 920–924.
88. Prado-Martinez J, Sudmant PH, Kidd JM, Li H, Kelley JL, et al. (2013) Great ape genetic diversity and population history. *Nature* .
89. Wu Y, Gusfield D (2007) Efficient computation of minimum recombination with genotypes (not haplotypes). *Journal of Bioinformatics and Computational Biology* : 181-200.
90. The 1000 Genomes Project Consortium (2010) A map of human genome variation from population-scale sequencing. *Nature* 467: 1061–1073.
91. Tavaré S (1984) Line-of-descent and genealogical processes, and their applications in population genetics models. *Theor Popul Biol* 26: 119–164.
92. Siepel A, Haussler D (2005) Phylogenetic hidden Markov models. In: Nielsen R, editor, *Statistical Methods in Molecular Evolution*, New York: Springer. pp. 325-351.
93. Felsenstein J, Churchill GA (1996) A hidden Markov model approach to variation among sites in rate of evolution. *Mol Biol Evol* 13: 93-104.
94. Rabiner LR (1989) A tutorial on hidden Markov models and selected applications in speech recognition. *Proceedings of the IEEE* 77: 257–286.
95. Durbin R, Eddy S, Krogh A, Mitchison G (1998) *Biological Sequence Analysis: Probabilistic Models of Proteins and Nucleic Acids*. Cambridge, UK: Cambridge University Press.
96. Cawley SL, Pachter L (2003) HMM sampling and applications to gene finding and alternative splicing. *Bioinformatics* 19 Suppl 2: II36-II41.
97. Zhu J, Liu JS, Lawrence CE (1998) Bayesian adaptive sequence alignment algorithms. *Bioinformatics* 14: 25–39.
98. International HapMap Consortium, Frazer KA, Ballinger DG, Cox DR, Hinds DA, et al. (2007) A second generation human haplotype map of over 3.1 million snps. *Nature* 449: 851–861.
99. Gronau I, Arbiza L, Mohammed J, Siepel A (2013) Inference of natural selection from interspersed genomic elements based on polymorphism and divergence. *Mol Biol Evol* 30: 1159–1171.
100. Tishkoff SA, Reed FA, Ranciaro A, Voight BF, Babbitt CC, et al. (2007) Convergent adaptation of human lactase persistence in Africa and Europe. *Nat Genet* 39: 31–40.

Data set	$n$	$L$	$M$	$\mu \times 10^8$	$\rho \times 10^8$	$\mu/\rho$	$N$
#1	20	1 Mb	100	2.5	{0.375, 0.75, 1.125, 1.50}	{6.67, 3.33, 2.22, 1.67}	10,000
#2	20	1 Mb	100	2.5	1.25	1.67	{2,500, 5,000, 7,500, 10,000}
#3	20	1 Mb	100	2.5	{0.417, 0.625, 1.25, 2.5}	{6, 4, 2, 1}	10,000

Table 1: **Summary of simulated data sets.**  $n$ : number of (haploid) sequences,  $L$ : length,  $M$ : number of replicates per parameter setting,  $\mu$ : mutation rate per site per generation,  $\rho$ : recombination rate per site per generation.

Annotation	Fold Enrichment	<i>P</i> -value
CDS	1.95	<0.001
Exon	1.75	<0.001
UTR	1.64	<0.001
Transcribed	1.41	<0.001
TSSProximal	1.25	0.001
Intronic	1.08	0.007
Promoter	0.97	0.657
Enhancer	0.74	>0.999
Insulator	0.68	>0.999
Intergenic	0.66	>0.999
Repeat	0.11	0.189

Table 2: **Enrichment of annotation classes in regions with extremely recent times to most recent common ancestry.** A threshold of 20,000 generations was applied to the posterior expected times to most recent common ancestry (TMRCA) computed from the *ARGweaver* samples based on genome-wide sequence data for 54 individuals. This produced a set of “recent TMRCA” genomic regions, which could be intersected with various annotation sets. *P*-values were computed by randomly shuffling the recent TMRCA regions, while maintaining their length properties (1000 replicates) and observing the numbers of bases that fall in each annotation class by chance. CDS: coding sequence, UTR: untranslated region, TSSProximal: proximal to (within 1 kb of) transcription start site.

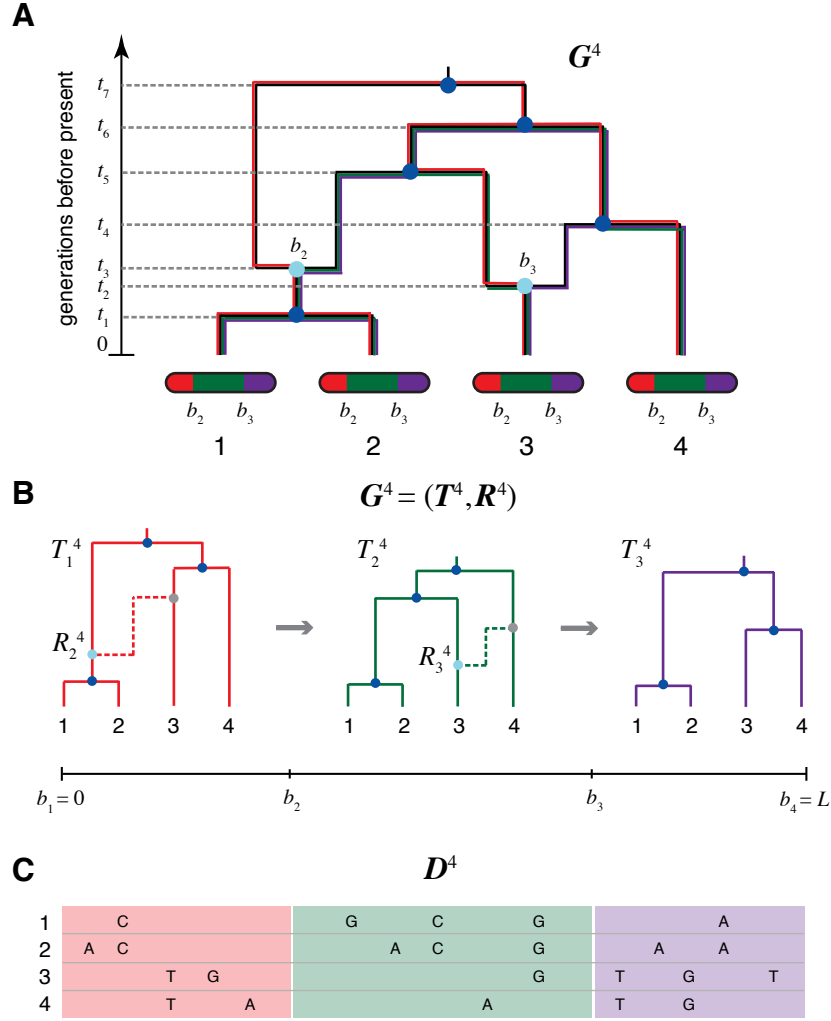


**Figure 1: An ancestral recombination graph (ARG) for four sequences.** (A) Going backwards in time (from bottom to top), the graph shows how lineages that lead to modern-day chromosomes (bottom) either “coalesce” into common ancestral lineages (dark blue circles), or split into the distinct parental chromosomes that were joined (in forward time) by recombination events (light blue circles). Each coalescence and recombination event is associated with a specific time (dashed lines), and each recombination event is also associated with a specific breakpoint along the chromosomes (here,  $b_2$  and  $b_3$ ). Each non-recombining interval of the sequences (shown in red, green, and purple) corresponds to a “local tree” embedded in the ARG (shown in matching colors). Recombinations cause these trees to change along the length of the sequences, making the correlation structure of the data set highly complex. The ARG for four sequences is denoted  $G^4$  in our notation. (B) Representation of  $G^4$  in terms of a sequence of local trees  $T^4$  and recombination events  $R^4$ . A local tree  $T_i^4$  is shown for each nonrecombining segment in colors matching those in (A). Each tree,  $T_i^4$ , can be viewed as being constructed from the previous tree,  $T_{i-1}^4$ , by placing a recombination event along the branches of  $T_{i-1}^4$  (light blue circles), breaking the branch at this location, and then allowing the broken lineage to re-coalesce to the rest of the tree (dashed lines in matching colors; new coalescence points are shown in gray). Together, the local trees and recombinations provide a complete description of the ARG. The Sequentially Markov Coalescent (SMC) approximate the full coalescent-with-recombination (CwR) by assuming that  $T_i^n$  is statistically independent of all previous trees given  $T_{i-1}^n$ . (C) An alignment of four sequences,  $D^4$ , corresponding to the linearized ARG shown in (B). For simplicity, only the derived alleles at polymorphic sites are shown. The sequences are assumed to be generated by a process that samples an ancestral sequences from a suitable background distribution, then allows each nonrecombining segment of this sequence to mutate stochastically along the branches of the corresponding local tree. Notice that the correlation structure of the sequences is fully determined by the local trees; that is,  $D^n$  is conditionally independent of the recombinations  $R^n$  given the local trees  $T^n$ .

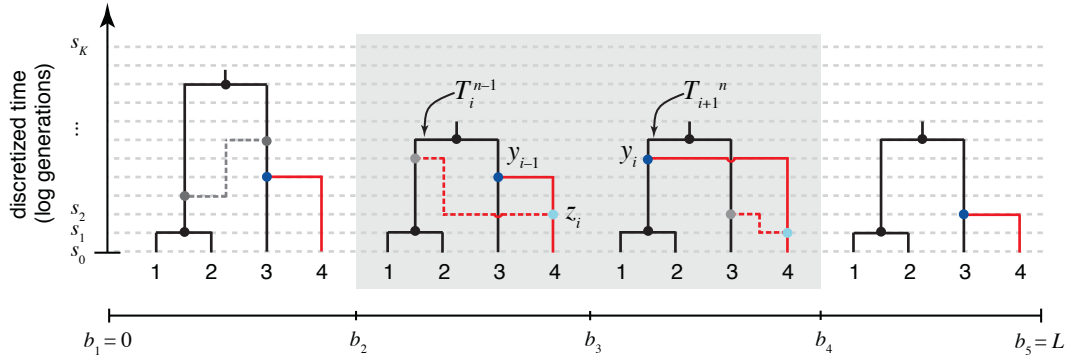


Figure 2: **The “threading” operation.** The threading operation adds an  $n$ th sequence to an ARG of  $n - 1$  sequences under a discretized version of the SMC (the DSMC) that requires all coalescence and recombination events to occur precisely at pre-defined time points,  $s_0, \dots, s_K$  (horizontal dashed lines). In this example, the 4th sequence has been removed from ARG  $G^4$  from Figure 1B, leaving a tree with  $n - 1 = 3$  leaves at each position  $i$  ( $T_i^{n-1}$ ). The fourth sequence (now shown in red) is re-threaded through the remaining portion of the ARG by first sampling a coalescence point  $y_i$  for this sequence at each  $T_i^{n-1}$ , thereby defining a new tree  $T_i^n$ , and then sampling a recombination point  $z_i$  to reconcile each adjacent pair of trees,  $(T_{i-1}^n, T_i^n)$ . For simplicity, only the distinct local trees for the four nonrecombining segments (after threading) are shown. The gray box highlights the pair of trees immediately flanking the breakpoint  $b_3$ . Notice that the first recombination from Figure 1B is retained (dark gray nodes and dashed line in left-most tree). In general, new recombinations are prohibited at the locations of “given” recombinations  $R^{n-1}$  (see text). Note that it is possible for the position of the  $n$ th sequence in the local trees to move due to old recombinations as well as new ones (not shown in this example).

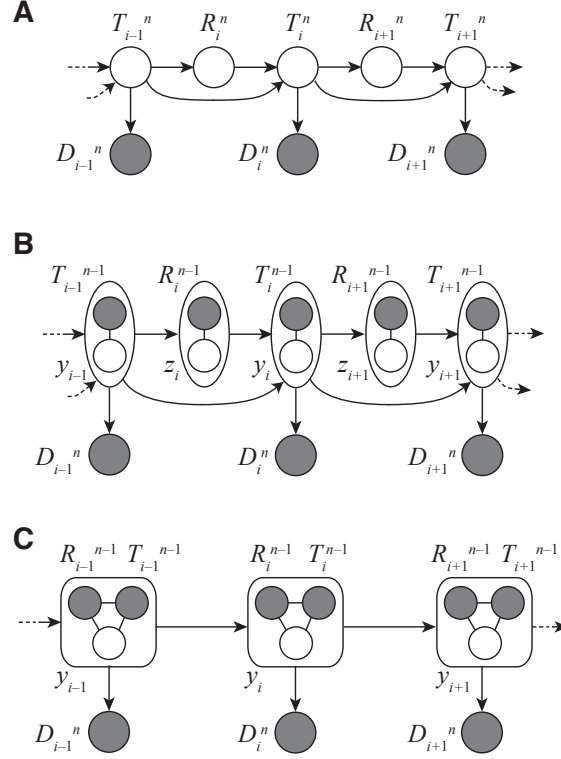


Figure 3: **Graphical models for Discretized Sequentially Markov Coalescent (DSMC) models.** (A) Full DSMC model for  $n$  samples with local trees,  $\mathbf{T}^n = (T_1^n, \dots, T_L^n)$ , recombinations,  $\mathbf{R}^n = (R_1^n, \dots, R_L^n)$ , and alignment columns,  $\mathbf{D}^n = (D_1^n, \dots, D_L^n)$ . Together,  $\mathbf{T}^n$  and  $\mathbf{R}^n$  define an ancestral recombination graph,  $\mathbf{G}^n$ . Solid circles indicate observed variables and empty circles indicate latent variables. Arrows indicate direct dependencies between variables and correspond to conditional probability distributions described in the text. Notice that the  $R_i^n$  variables can be integrated out of this model, leading to the conventional graph topology for a hidden Markov model. (B) The same model as in (A), but now partitioning the latent variables into components that describe the history of the first  $n-1$  sequences ( $\mathbf{T}^{n-1}$  and  $\mathbf{R}^{n-1}$ ) and components specific to the  $n$ th sequence ( $\mathbf{Y} = (y_1, \dots, y_L)$  and  $\mathbf{Z} = (z_1, \dots, z_L)$ ). The  $\mathbf{T}^{n-1}$  and  $\mathbf{R}^{n-1}$  variables are shown as solid nodes because they are now “clamped” at specific values. A sample of  $(\mathbf{Y}, \mathbf{Z})$  represents a threading of the  $n$ th sequence through the ARG. (C) Reduced model after elimination of  $\mathbf{Z}$  by integration, enabling efficient sampling of coalescent threadings  $\mathbf{Y}$ . The grouped nodes have complex joint dependencies, leading to a heterogeneous state space and normalization structure, but the linear conditional independence structure of an HMM is retained.

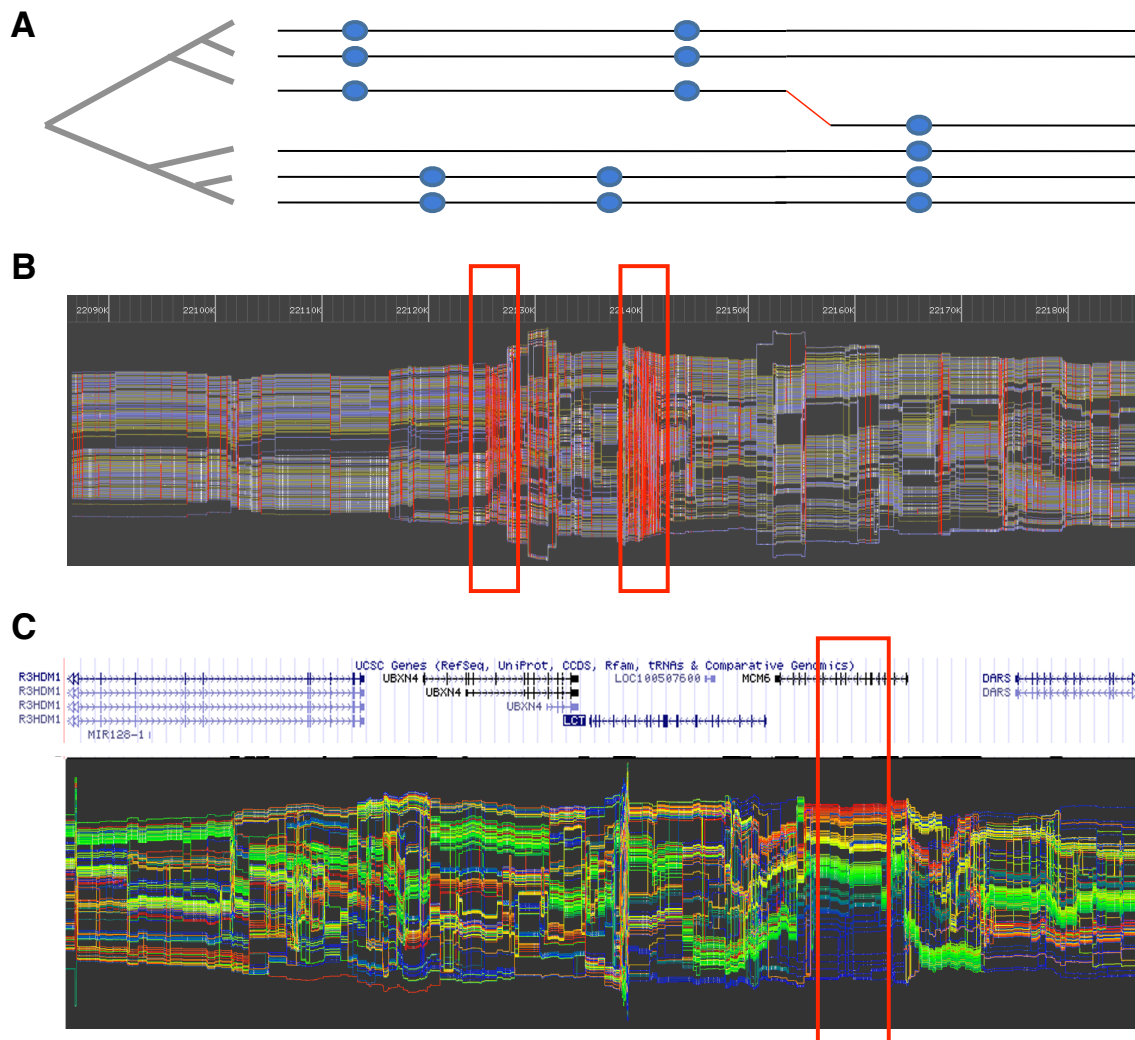


Figure 4: “**Leaf trace**” visualization of inferred ancestral recombination graphs. (A) Each haploid sequence in the sample is represented by a line, and these lines are ordered and spaced according to the local tree at each position. Spacing between adjacent lines reflects time to most recent common ancestry of associated sequences. Nonrecombining genomic intervals are reflected by blocks of parallel lines, and recombinations lead to changes in spacing and/or order (highlighted in red). Hypothetical polymorphisms are shown (blue circles = derived alleles) to indicate the data driving the inference. Notice that aspects of the leaf ordering are arbitrary, because the two children between each ancestral node can be exchanged without altering the meaning of the diagram. (B) Leaf trace for real data from Complete Genomics. Dense clusters of crossing lines (red boxes) reflect recombination hot spots, while long blocks of parallel lines reflect cold spots. (C) Lines colored in rainbow pattern at a particular locus of interest highlight decay of haplotype structure around that locus. Here the diagram is centered on the promoter region of the lactase (LCT) gene. The conserved haplotype block around this region (red box) evidently reflects selective sweeps in human populations [100].



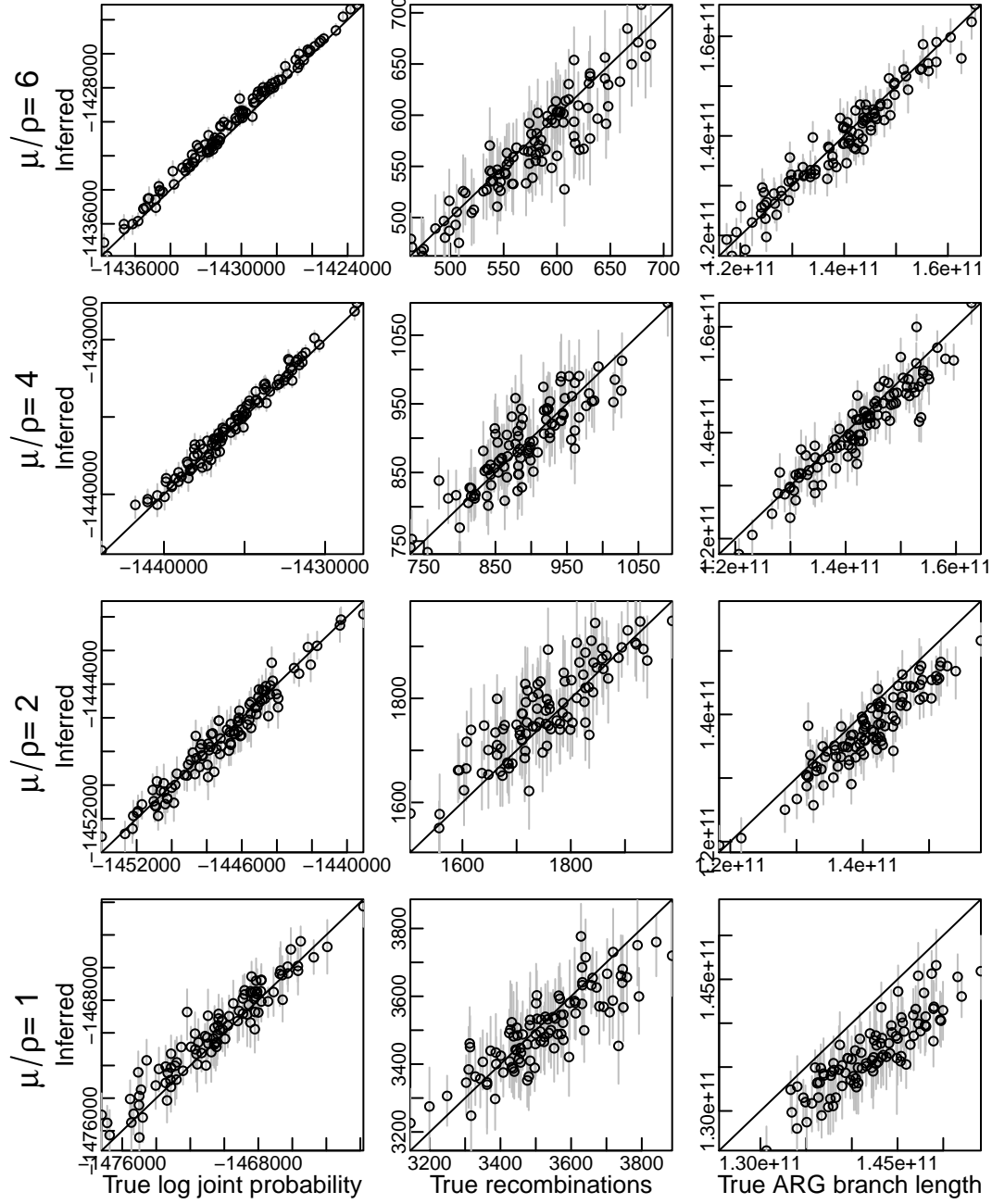


Figure 5: **Application of ARGweaver to simulated data.** Using the coalescent-with-recombination, we simulated 100 datasets each with 20 1 Mb haplotypes sampled from a population with effective size  $N = 10,000$  and a mutation rate of  $\mu = 2.5 \times 10^{-8}$  mutations/site/generation. The recombination rate was varied as a fraction of the mutation rate (rows; see data set #3 in Table 1). ARGweaver was able to recover several properties of the ARG with reasonable accuracy over a range of ratios of mutation to recombination rates ( $\mu/p$ ), including the log joint probability (the logarithm of equation 16), the number of recombinations, and the total branch length of the ARG (columns, left to right). Notice that the total branch length of the ARG exhibits some downward bias at low values of  $\mu/p$ . Circles represent averages across 100 sampled ARGs, sampled at intervals of 10 after a burn-in of 200 iterations, and error bars represents a 95% confidence intervals (interpretable as posterior expected values and Bayesian credible intervals in columns 2 and 3).

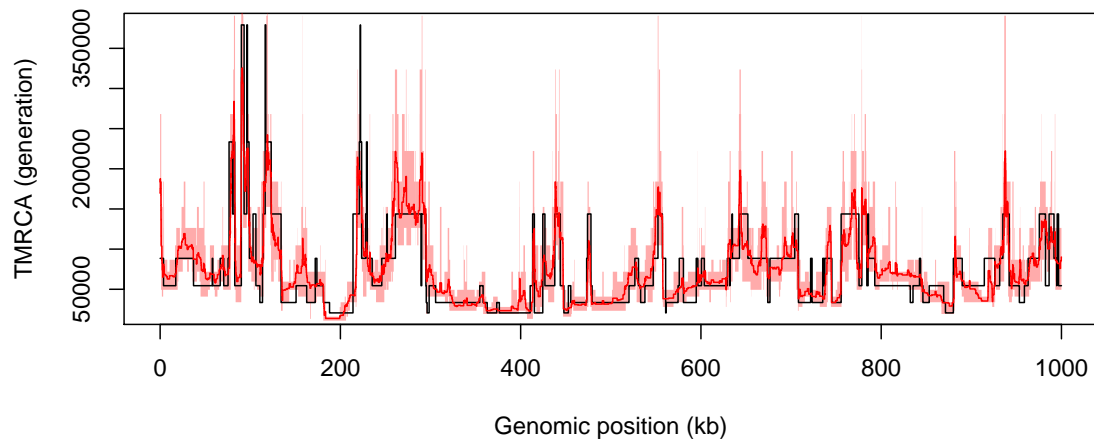


Figure 6: **Recovery of time to most recent common ancestor in simulated data.** The posterior mean estimate of the TMRCA (red line, with 95% credible intervals in light red) closely follows the true TMRCA in data simulated under the coalescent-with-recombination (data set #3 with  $\mu/\rho = 6$ , Table 1; black line).

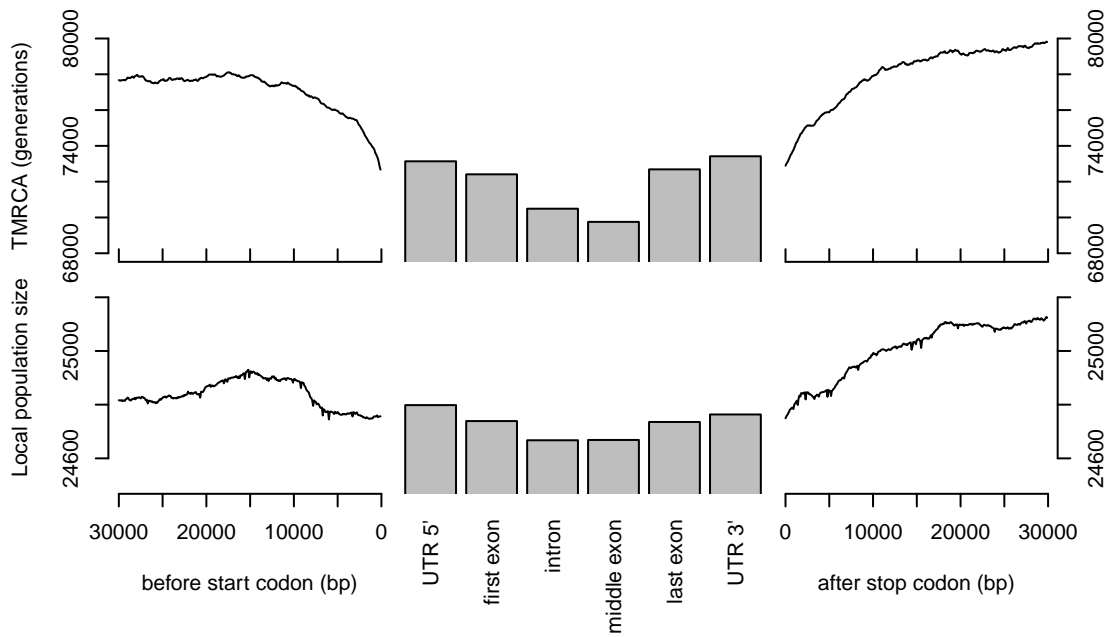
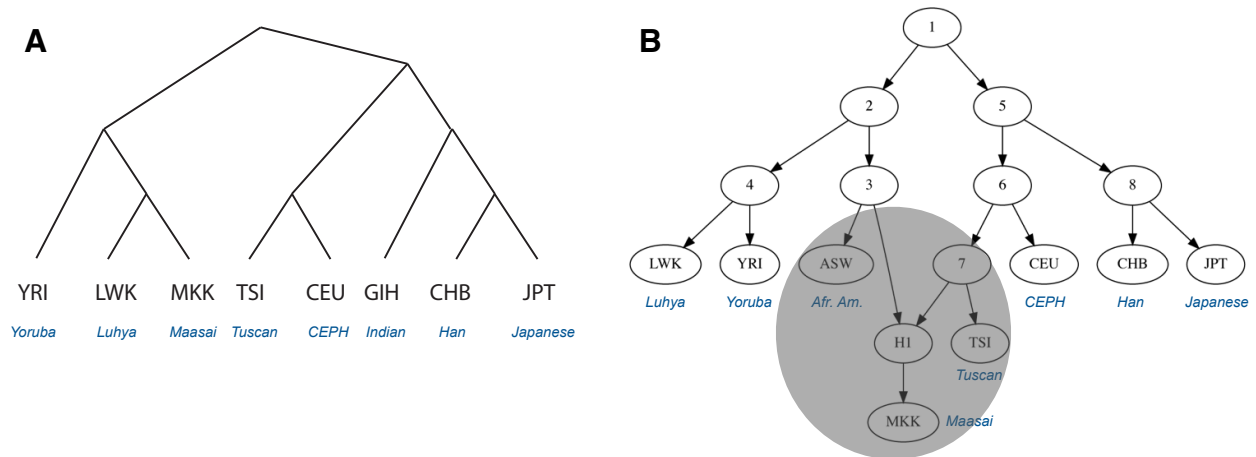
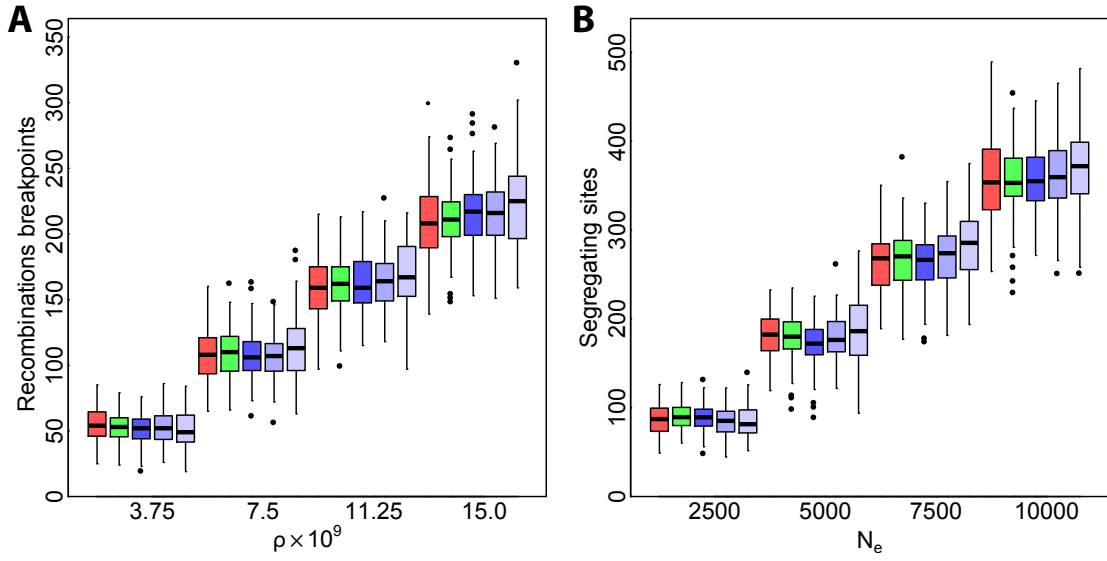


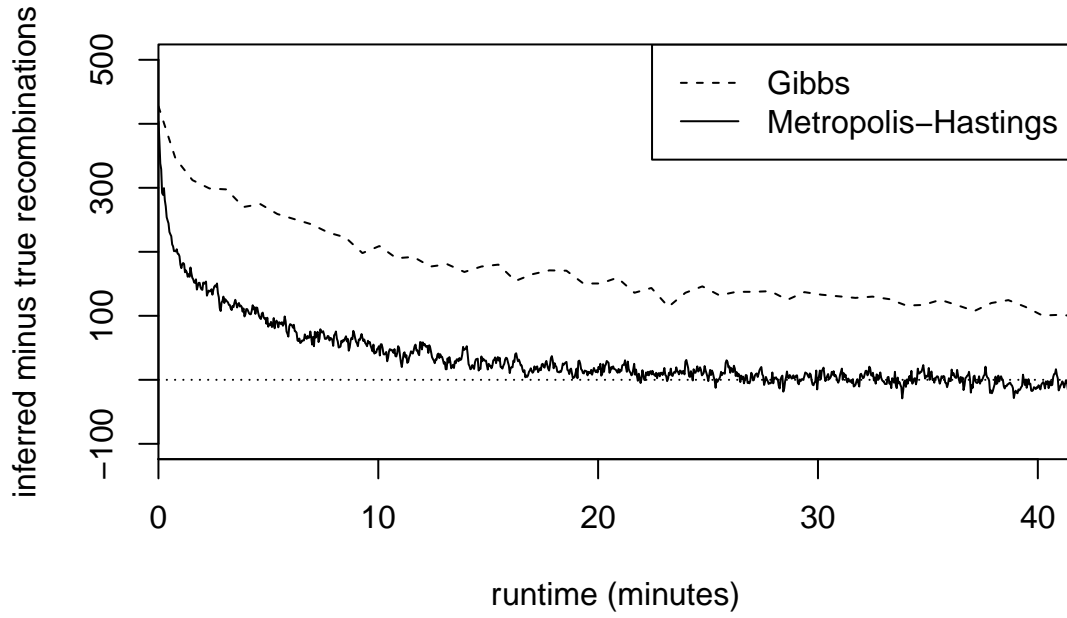
Figure 7: **Average TMRCA and local effective population size near protein coding genes.** Values represent position-specific averages over all genes considered. Ancestral recombination graphs were inferred from 54 human genome sequences from Complete Genomics (see text). The estimated values were similar within each component of the gene body (bars) so were further averaged across positions within each of these classes. UTR: untranslated region. Here “exon” indicates coding portions of exons only.



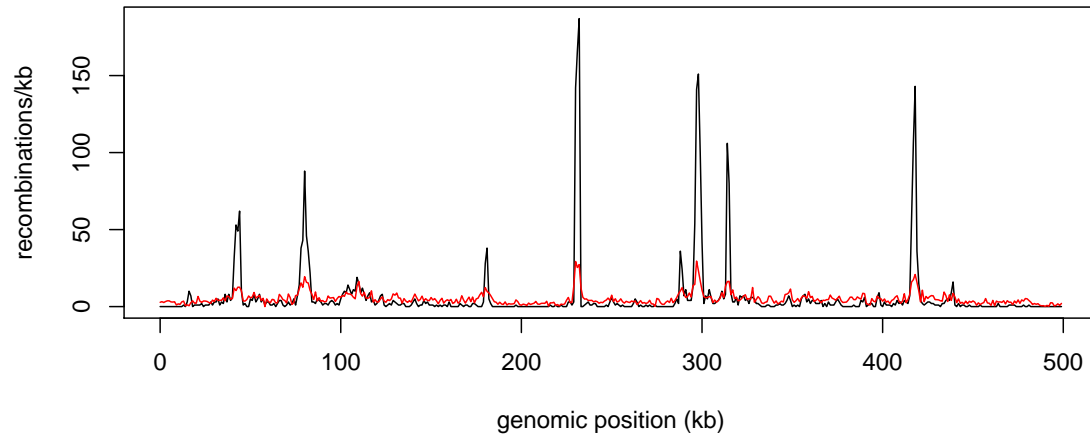
**Figure 8: Human population phylogenies based on local trees from the sampled ancestral recombination graphs.** (A) Phylogeny for eight populations that exhibit limited admixture, inferred using the Minimizing Deep Coalescences (MDC) algorithm implemented in PhyloNet, which attempts to explain differences between the population phylogeny and the local trees in terms of incomplete lineage sorting [65]. This method recovered the expected phylogeny. Data was from Complete Genomics (see text). (B) Phylogeny for seven of the eight populations in (A) plus the admixed African American population (ASW), inferred using an algorithm, also implemented in PhyloNet, that allows for hybridization as well as incomplete lineage sorting [67]. This method recovered most of the phylogeny and correctly identified the presence of admixture but was unable to correctly resolve the relationships among the affected populations (region highlighted in gray; see text). In this diagram, numbered nodes represent nonadmixed ancestral populations, and H1 is an ancestral hybrid population.



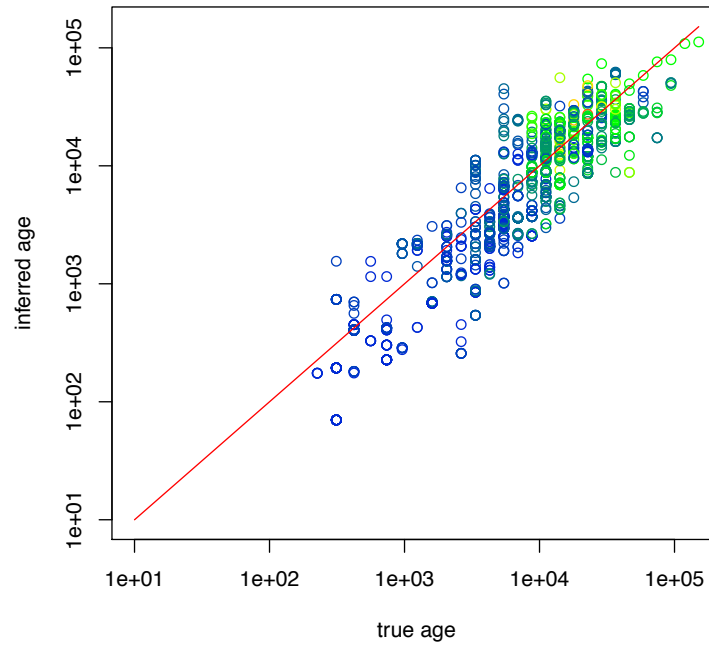
Supplementary Figure S1: **ARGs simulated under Discretized Sequentially Markov Coalescent model are similar to those simulated under continuous models.** ARGs were simulated using the coalescent-with-recombination (red), Sequentially Markov Coalescent (green), and Discretized Sequentially Markov Coalescent (blue). Three versions of the DSMC were considered: ones with with  $K = 40$  (dark blue),  $K = 20$  (medium blue), and  $K = 10$  (light blue) time intervals. In all cases, we assumed  $s_K = 200,000$  generations. (A) Numbers of recombinations at four different recombination rates. To make the comparison fair, recombinations between nonancestral sequences (which are disallowed by the SMC/DSMC) are excluded in the case of the coalescent-with-recombination. However, “diamond” or “bubble” recombinations (ones that are immediately reversed by coalescence events, going backwards in time) were included, so any distortion from excluding these events in the SMC/DSMC is reflected in the figure. (B) Numbers of segregating sites at four different effective population sizes.



Supplementary Figure S2: **Convergence of *ARGweaver* with simulated data.** When the number of sequences exceeds 6–8, the Metropolis-Hastings algorithm and subtree threading operation are needed for *ARGweaver* to have acceptable convergence properties. These data are based on simulated data set #3 with  $\mu/\rho = 2$  (Table 1). Here the measure of convergence is the difference between the number of inferred recombination events and the number of true recombination events. Other measures show similar patterns.

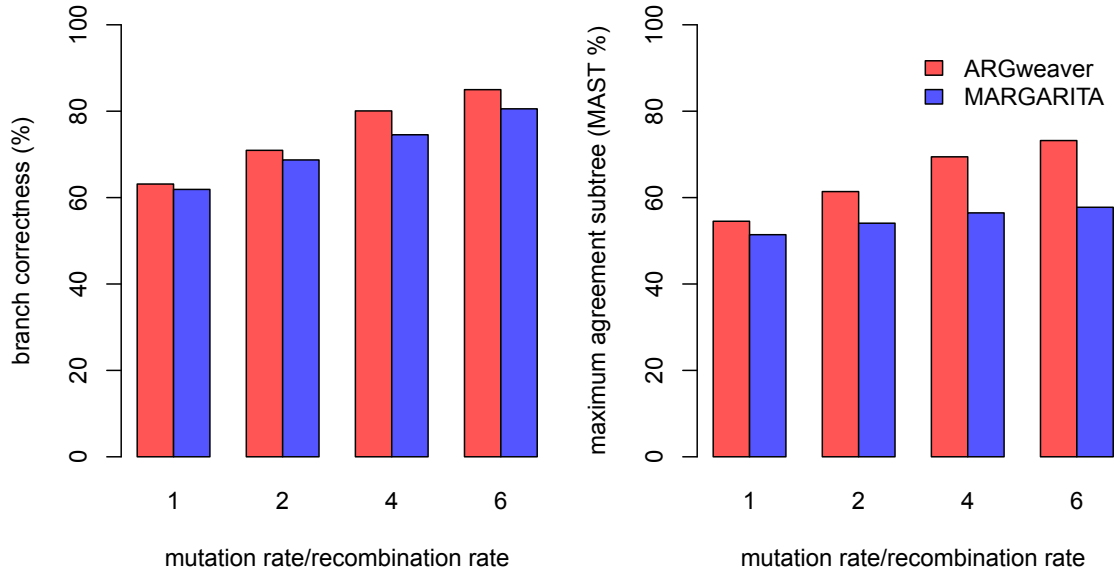


Supplementary Figure S3: **Recovery of recombination rates from simulated data.** Using variable recombination rates as found in the human genome, we simulated an alignment of 100 sequences with  $N = 20,000$  and  $\mu = 1.2 \times 10^{-8}$ . Despite the assumption in the prior of a constant recombination rate of  $\rho = 1.16 \times 10^{-8}$ , the posterior mean estimate of the average number of recombinations in a 1 kb sliding window (red line) correlates well with the true recombination rates (black line). Notice that recombination hotspots are clearly identifiable by peaks in the inferred rates but the magnitudes of these peaks are dampened by the use of a uniform prior. Only recombinations that produced changes in tree topology (the class that is detectable by our methods) were considered.

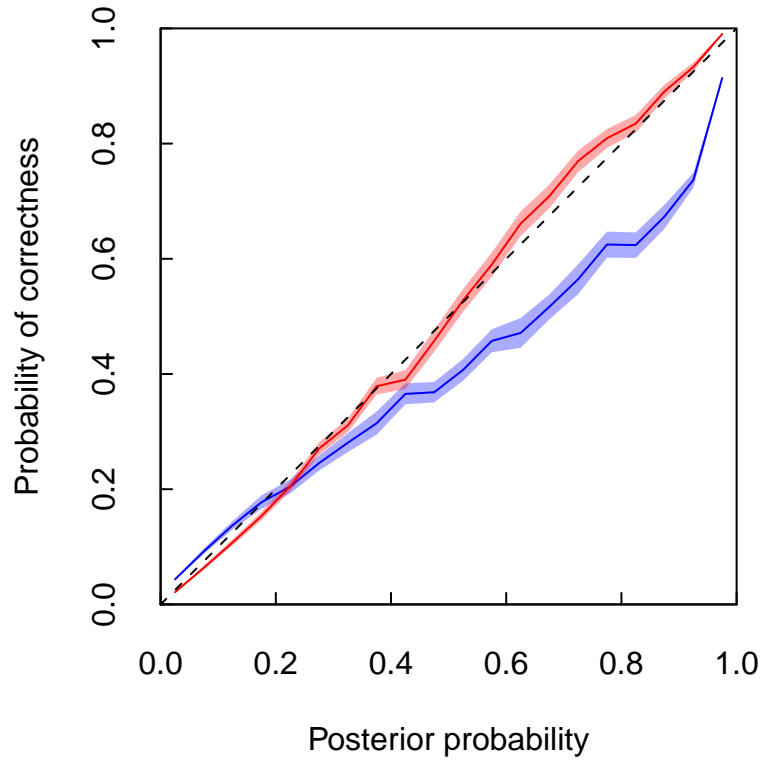


Supplementary Figure S4: **True vs. estimated ages of derived alleles in simulated data.** Ages were estimated by calculating the midpoint of the branch on which the mutation was inferred to occur, under an infinite sites model, and averaging across sample from the posterior distribution. Points are colored on a spectrum from blue to green in proportion to derived allele frequencies. Notice that younger alleles tend to have lower frequencies and older alleles tend to have higher frequencies, but the correlation is imperfect. The ARG enables much better estimates of allele age than allele frequencies alone. Ages are measured in generations before the present.

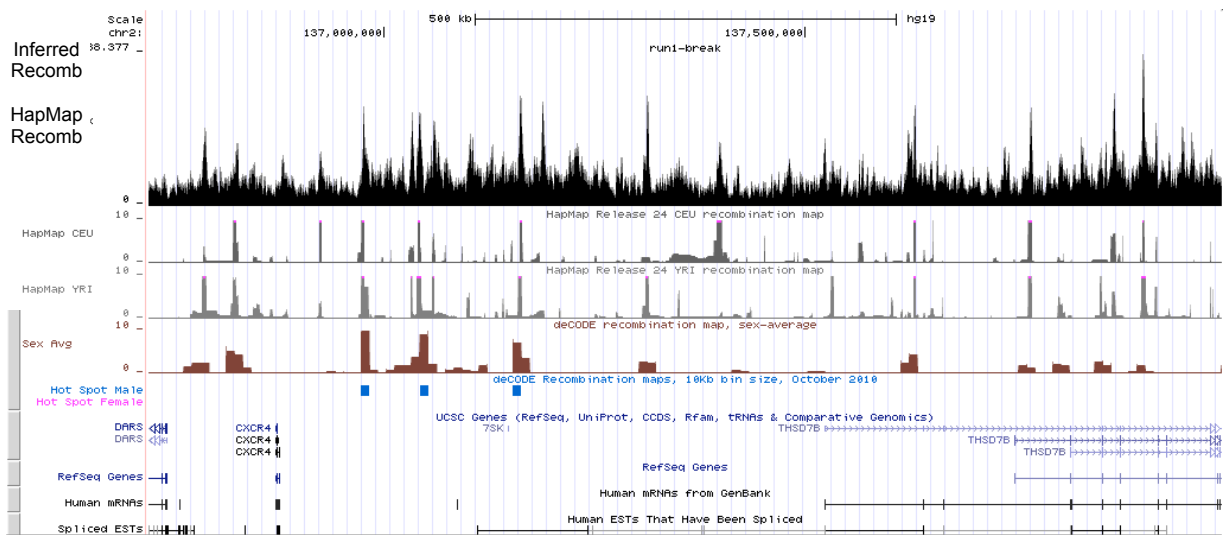




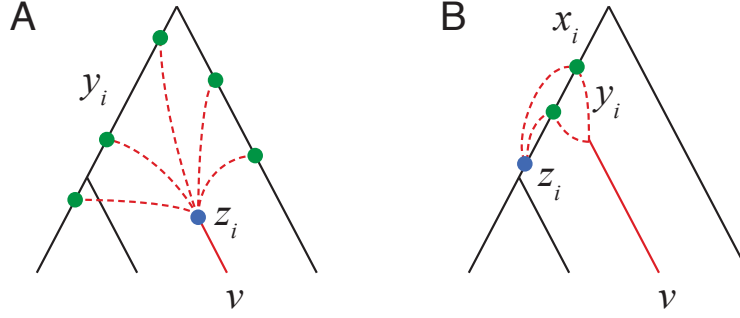
Supplementary Figure S5: **Recovery of local tree topologies.** Sequences were simulated under the coalescent-with-recombination (data set #3, Table 1), ARGs were inferred using *ARGweaver*, then 100 equally spaced local trees were extracted from the sampled ARGs. The topologies of these trees were compared with the true trees generated during simulation at corresponding positions in the alignment. We compared *ARGweaver* with the heuristic *Margarita* program [34] by two measures: (A) branch correctness (one minus the normalized Robinson-Foulds (RF) distance [59]) and (B) Maximum Agreement Subtree (MAST) percentages (the size of the largest leaf-set such that induced subtrees are topologically equivalent, expressed as a percentage of the total number of leaves), across a range of mutation to recombination rate ratios ( $\mu/\rho$ ). In all cases, *ARGweaver* produced significantly more accurate trees.



Supplementary Figure S6: **Local tree branch posterior probabilities inferred by *ARGweaver* accurately reflect their probability of correctness.** The branch posterior probabilities found by *ARGweaver* (red) more accurately reflect the probability of the branch being correct than the frequency at which *Margarita* (blue) infers a branch. For each method, branches were binned by their posterior probability (windows of 5%) and compared against their frequency of branch correctness. Shaded regions represent the 95% binomial confidence interval. This plot is based on simulated data set #3 (Table 1) with  $\mu/\rho = 6$ . Posterior probabilities for *ARGweaver* are based on 1000 samples from the Markov chain, and the probabilities for *Margarita* reflect 100 independent samples.



Supplementary Figure S7: **Recombination rates inferred from real data.** Inference is based on data from Complete Genomics (see text). Notice that spikes in inferred recombination rates (top plot, in black) correspond reasonably well with recombination hot spots (tracks at bottom).



Supplementary Figure S8: **Cases for new recombination  $z_i$  given re-coalescence point  $y_i$ .** (A) In the main case, the recombination  $z_i$  (blue point) occurs on the branch that is being threaded into the ARG ( $v$ ; shown in red). After a recombination on this branch, a re-coalescence can occur at any point  $y_i$  (green points) in the local tree  $T_i^{n-1}$  such that  $y_i$  is at least as old as  $z_i$ . Therefore, when enumerating the possible  $z_i$  consistent with a given  $y_i$ , one must consider all points on branch  $v$  at least as recent as  $y_i$ . This set is denoted  $Z_1$  in the text. (B) There is an additional special case to consider when branch  $v$  coalesces to the same branches of  $T_i^{n-1}$  at positions  $i-1$  and  $i$ , that is, when  $x_{i-1} = x_i$ . In this case, it is possible that the recombination  $z_i$  (blue point) occurs not on the new branch  $v$  but on  $x_i$  (black branch) at a time point no older than the re-coalescence time  $y_i$  (green points). A recombination of this kind will leave an identical signature to the symmetric case of a recombination on  $v$  in the same time interval followed by a re-coalescence of  $v$  to  $x_i$ . Therefore, when enumerating the possible  $z_i$  consistent with a given  $y_i$  such that  $x_{i-1} = x_i$ , one must also consider the set  $Z_2$  consisting of all  $z_i$  on  $x_i$  such that  $z_i$  is at least as recent as  $y_i$ . Notice that, in both (A) and (B), the tree excluding  $v$  is unchanged by all recombination and coalescence scenarios  $(z_i, y_i)$  under consideration, i.e.,  $T_{i-1}^{n-1} = T_i^{n-1}$  (black branches).